ANKARA YILDIRIM BEYAZIT UNIVERSITY

GRADUATE SCHOOL OF NATURAL AND APPLIED SCIENCES

STRAIGHTENER DESIGN AND ANALYSIS FOR AIR CONDITIONING SYSTEM AIR DISTRIBUTION DUCTING OF A ROTORCRAFT

M.Sc. Thesis by

Mert ÇEKÜÇ

Department of Aerospace Engineering

April, 2023

ANKARA

STRAIGHTENER DESIGN AND ANALYSIS FOR AIR CONDITIONING SYSTEM AIR DISTRIBUTION DUCTING OF A ROTORCRAFT

A Thesis Submitted to

The Graduate School of Natural and Applied Sciences of

Ankara Yıldırım Beyazıt University

In Partial Fulfillment of the Requirements for the Degree of Master of Science in Aeronautics and Astronautics, Department of Aerospace Engineering

by

Mert ÇEKÜÇ

April, 2023

ANKARA

M.Sc. THESIS EXAMINATION RESULT FORM

We have read the thesis entitled **"STRAIGHTENER DESIGN AND ANALYSIS FOR AIR CONDITIONING SYSTEM AIR DISTRIBUTION DUCTING OF A ROTORCRAFT"** completed by **MERT ÇEKÜÇ** under the supervision of **ASSOC. PROF. DR. MUNIR ELFARRA** and we certify that in our opinion it is fully adequate, in scope and in quality, as a thesis for the degree of Master of Science.

Assoc. Prof. Dr. Munir ELFARRA

Supervisor

Dr. Orhan ÖZÇELİK

Jury Member

Dr. Mohamed S. ELMNEFI

Jury Member

Prof. Dr. Sadettin ORHAN

Director

Graduate School of Natural and Applied Sciences

ETHICAL DECLARATION

I hereby declare that, in this thesis which has been prepared in accordance with the Thesis Writing Manual of Graduate School of Natural and Applied Sciences,

- All data, information and documents are obtained in the framework of academic and ethical rules,
- All information, documents and assessments are presented in accordance with scientific ethics and morals,
- All the materials that have been utilized are fully cited and referenced,
- No change has been made on the utilized materials,
- All the works presented are original,

and in any contrary case of above statements, I accept to renounce all my legal rights.

Date: 2023, 24 April **Signature: ……..**

Name & Surname: Mert ÇEKÜÇ

ACKNOWLEDGEMENTS

Firstly, I would like to express my sincere gratitude to my supervisor, Assoc. Prof. Dr. Munir Elfarra for his tremendous support and motivation during my study. His immense knowledge and precious recommendations constituted the milestones of this study. His guidance assisted me all the time of my research and while writing this thesis. I would like to thank my friends and family who supported me during this study. Finally, I would like to dedicate all my work to my mother and father.

April, 2023 **Mert ÇEKÜÇ**

STRAIGHTENER DESIGN AND ANALYSIS FOR AIR CONDITIONING SYSTEM AIR DISTRIBUTION DUCTING OF A ROTORCRAFT

ABSTRACT

The Rotorcraft Air Conditioning System aims to provide a comfortable thermal environment for the crew and the passengers. According to aviation standards, the minimum required amount of fresh air for crew and passengers shall be provided to cockpit and cabin zones during all flight phases. The systems consist of many equipment and air distribution ducting package that varies depending on the air conditioning methods, and installation location on the rotorcraft. They include at least one fan and low-pressure air distribution ducting. Air ducts have long routing, variable cross sections, and diameter values. The fans consist of two sections, rotor and stator. The stator straightens the flow. However, they are not sufficient to smooth the airflow in the rotorcraft air distribution ducting system. Therefore, the airflow straighteners are used to provide uniform air distribution in the cockpit air distribution ducting. The straighteners are designed depending on the air distribution ducting routing, although there are identified many different types like zanker, fin, vortab for them.

In this study, the air distribution ducting, installed and has been used in the helicopter, is improved by using the airflow straighteners to provide equivalent air mass flow rate from all air outlets. Initially, air velocity values on each air outlet are measured as experimental at different rotational fan speeds. Tested air distribution ducting is created and simulated by using Star CCM+. Then, the new straighteners are designed via 3-D programs and the calculations are utilized using computational fluid dynamics (CFD). Results of all CFD studies are compared and one straightener design is suggested for the rotorcraft.

Keywords: Air conditioning system, air distribution ducting, air flow, air flow straightener, air flow conditioner, fan, blades, air velocity.

HELİKOPTER İKLİMLENDİRME SİSTEMLERİNDEKİ HAVA DAĞITIM KANALLARI İÇİN AKIŞ DÜNLEYİCİSİ TASARIMI VE ANALİZİ

ÖZ

Helikopter iklimlendirme sistemleri yolcular ve kabin görevlileri için termal olarak konforlu ortam sağlamayı amaçlamaktadır. Havacılık standartlarına göre, tüm uçuş fazları süresince, sürekli minimum gerekli olan taze hava miktarı kadar hava sağlanması gerekmektedir. Sistemler, kullanılan iklimlendirme sistemi yöntemine ve hava aracı üzerindeki yerleşimine bağlı olarak birçok ekipman ve hava kanal paketlerinden oluşmaktadır. Bu sistemler en az bir adet fandan ve alçak basınç hava dağıtım kanallarından içerir. Hava kanalları uzun rotalamalara, değişken kesit alanlarına ve çap değerlerine sahiptir. Fanlar, rotor ve stator olmak üzere iki bölümden oluşur. Stator, akış düzenleyicidir. Fakat, stator helikopterlerdeki hava kanallarındaki akışı düzleştirme konusunda verimli değildir. Bu yüzden, kokpit hava dağıtım kanalında uniform akış dağılımı sağlamak için akış düzenleyicisi kullanılır. Akış düzenleyiciler için tanımlanmış zanker, fin, vortab gibi birçok farklı tiplerinin olmasına rağmen akış düzenleyiciler hava dağıtım kanalların rotasına bağlı olarak tasarlanır.

Bu çalışmada, helikoptere entegre edilmiş ve kullanılan hava dağıtım kanalları, tüm hava çıkışlarından özdeş hava debisi sağlamak amacıyla, akış düzenleyiciler kullanılarak geliştirilmiştir. İlk olarak, deneysel olarak farklı fan hızlarında, her bir hava çıkışındaki hız değerleri ölçülmüştür. Testlerde kullanılan geometri üç boyutlu ortamlar oluşturulmuş ve StarCCM+ aracılığı ile modellenmiştir. Sonrasında, üç boyutlu programlar aracılığı ile yeni akış düzenleyiciler tasarlanmış ve hesaplamalı akışkanlar mekaniği kullanılarak hesaplamalar yapılmıştır. Bu hesaplamaların sonuçları karşılaştırılmış ve bir akış düzenleyicisi tasarımı önerilmiştir.

Anahtar Kelimeler: İklimlendirme Sistemi, hava dağıtım kanalları, hava akışı, akış düzenleyici, akış kısıtlayıcı, fan, kanatçıklar, hava hızı.

NOMENCLATURE

ANS American Nuclear Society

ANSI American National Standards Institute

ASHRAE American Society of Heating, Refrigerant and Air Conditioning Engineers

CFD Computational Fluid Dynamics

CS Certification Specification

DC Direct Current

DES Detached Eddy Simulation

ECS Environmental Control System

HVAC Heating, Ventilation and Air Conditioning

IFMIF International Fusion Materials Irradiation Facility

LES Large Eddy Simulations

MRF Multiple Rotating Reference Frame

RANS Reynolds Averaged Navier Stokes

PF Profile Factor

Phd Philosophie Doctor

RSM Reynolds Stress Model

CONTENTS

LIST OF TABLES

LIST OF FIGURES

CHAPTER 1

INTRODUCTION

An Environmental Control System in a rotorcraft, such as a helicopter, is designed to regulate the temperature and humidity inside the cabin, ensuring a comfortable environment for the passengers and crew. The system typically consists of several components, including an air conditioning unit, air distribution ducting subsystem, a ventilation subsystem, and a heating subsystem.

There are using two different methods, air cycle and vapor compression cycle for air conditioning units. The vapor cycle system typically consists of an air compressor, a condenser, an expansion valve, an evaporator, and a refrigerant. The compressor compresses the refrigerant, which then moves through the condenser where it releases heat and turns into a high-pressure, high-temperature liquid. The liquid goes to the expansion valve to decrease the refrigerant temperature. However, the phase of the refrigerant is changed from liquid to liquid-vapor mixture due to the expansion valve. The liquid then moves through the evaporator where it absorbs heat from the air inside the cabin and cockpit, turning back into a low-pressure, low-temperature gas. This cooled air is then circulated throughout the cabin and cockpit throughout air distribution ducting to lower the temperature.

The heating subsystems work by circulating warm air through the cabin and cockpit, which can be generated by various heat sources, such as engine bleed air, electrical heaters, or a combination of both. The design of heating subsystems for rotorcraft can vary depending on the type of helicopter and its intended mission, but they generally include a heat exchanger, temperature control valves, and air distribution ducting to distribute the warm air throughout the cabin and cockpit. Additionally, some rotorcraft may also have systems in place to remove demist from the cockpit windows and other surfaces, which can be especially important in cold weather operations.

The ventilation subsystem provides fresh air to the cabin and cockpit and removes stale air and odors. According to the aviation standard, which is CS-29 Certification Specifications and Acceptable Means of Compliance for Large Rotorcraft [1], required

minimum fresh air per minute per crew/passengers shall be provided to the cabin and cockpit. Moreover, crew and passenger compartment air must be free from harmful or hazardous concentration under any reasonably probable failure of any subsystem or equipment. The ventilation subsystem shall be helpful to remove smoke from the cabin and cockpit.

An Air Distribution Ducting subsystem is designed to distribute conditioned air throughout the cabin and cockpit. The system typically consists of a series of ducts, vents, fans, and diffusers that transport air from the Environmental Control System (ECS) to different areas of the cabin and cockpit. The ducting is usually made of lightweight, durable materials such as aluminum or composites and is designed to withstand the high temperatures, pressures, and vibrations present in aircraft. The ducts are routed through the cabin and cockpit in such a way as to optimize the distribution of conditioned air and minimize the potential for leaks. The ducts also may include temperature and pressure sensors, valves, and actuators to control the flow of air and ensure proper cabin pressurization. Overall, the Air Distribution Ducting system plays a significant role in maintaining a comfortable and safe environment for passengers and crew during different flight conditions and different weather conditions by ensuring that the conditioned air reaches all areas of the cabin and cockpit.

The airflow straighteners are devices that are used to improve the performance of airflow subsystems by reducing turbulence and increasing airflow efficiency. They are used in a variety of applications, including HVAC systems, air-cooled heat exchangers, and industrial ducts. The use of airflow straighteners can result in significant energy savings, improved thermal comfort, and increased system efficiency.

Airflow straighteners have been studied extensively in the past decades, with research focusing on their design, performance, and application. Various types of airflow straighteners have been developed, including those made of porous materials, ribbed surfaces, and perforated plates. Airflow straighteners made of porous materials, such as metal foams and sintered metal plates, have been developed. These materials have small pores that allow air to pass through while reducing turbulence and increasing airflow efficiency. Airflow straighteners with ribbed surfaces, such as corrugated

sheets and wavy plates, have been developed. These devices use the ribbed surface to create vortices that help to reduce turbulence and increase airflow efficiency. Perforated plates are often used as airflow straighteners. These devices have small holes that allow air to pass through while reducing turbulence and increasing air flow efficiency. Vane-type airflow straighteners are devices that are made of thin vanes that are fixed to the duct walls. They act as a barrier for the turbulent flow and create vortices that help to reduce turbulence and increase air flow efficiency. Vortex generators are small devices that are used to create vortices in the air flow, which can help to reduce turbulence and increase air flow efficiency. Coanda effect-based flow straighteners are devices that use the Coanda effect to create a curved flow that can help to reduce turbulence and increase air flow efficiency.

A Zanker-type straightener, also known as a Zanker vortex generator, is a device that is used to create vortices in fluid flow in order to straighten and stabilize the flow. The Zanker type straightener is similar to other types of vortex generators, but it is designed specifically to straighten the flow of air or other gases. A Zanker-type straightener typically consists of a series of small plates or fins arranged in a specific pattern. The plates or fins are typically triangular in shape, with the tip of the triangle facing the fluid flow. The plates or fins can be made from a variety of materials, including metal, plastic, or composite materials. It is important to note that the Zanker-type straightener is most effective when the flow is turbulent, and the fluid is incompressible. The Zanker type straightener is typically used in conjunction with other flow control devices, such as diffusers, to achieve the desired flow characteristics.

These are some of the main types of air flow straighteners that have been developed. Each type has its own advantages and disadvantages, and the effectiveness of the device depends on various factors such as the type of air flow system and the specific application. Moreover, the effectiveness of air flow straighteners is typically evaluated by measuring the pressure drop across the device and the reduction in turbulence.

The thickness of an air flow straightener can have a significant impact on the performance of the airflow in a duct or pipe. Increasing the thickness of the straightener can reduce turbulence and improve the smoothness of the airflow. This can lead to an increase in pressure drop. Increasing the thickness of the straightener can also increase

the resistance to airflow, which can lead to a decrease in flow rate. This can negatively affect the performance of the system. In general, the optimal thickness of an air flow straightener will depend on the specific application and the characteristics of the airflow. For example, for high-velocity flows, a thicker straightener may be more effective in reducing turbulence, while for low-velocity flows, a thinner straightener may be more appropriate to avoid excessive pressure loss. Additionally, the thickness of the straightener will also depend on the materials and the design of the straightener. Some materials or designs may be more effective at reducing turbulence and improving airflow at a specific thickness than others. Overall, the effects of the straightener thickness on the airflow are complex and depend on various factors such as flow rate, pressure drop, and the characteristics of the airflow. It is important to consider these factors and conduct testing to determine the optimal thickness for a specific application.

In this study, air distribution ducting, located on a rotorcraft, is improved using a designed flow straightener under the defined constant temperature condition. Initially, air velocity values of each air outlet are measured at different rotational fan speeds via hot wire anemometers as experimental. Tested air distribution ducting is created via Catia V5-R22 and simulated by using Star CCM+. The simulations are conducted for one rotational fan speed to determine optimum mesh values. After the find optimum mesh, the simulations are conducted at three different fan speeds. Then, the air velocity values, taken from each air outlet on the simulations, are compared with the experimental studies. According to the comparison study, the required improvement for air velocity from the air outlets is decided and a perforated straightener is designed. The effect of increasing the diameter of holes on the straightener and changing of the thickness of the straightener on the air flow distribution in the ducting is investigated. As a result of this study, one straightener is proposed for the air distribution ducting in a helicopter.

1.1 Literature Review

Literature surveys are conducted to examine completed studies, to make an inference, to learn different flow conditioner types, and to investigate made calculations such as velocity, turbulence, and swirl angle via different portals. The found articles, the journals, the master thesis, the Ph.D. thesis, and the books are categorized as experimental studies, computational studies, and both experimental and numerical studies.

1.1.1 Experimental Studies

Captured total and three different tube bundles, a Zanker, and an etoile flow conditioner were tested by Brennan et all. In this study, tests were designed to find a location for the flow conditioner. Moreover, other aims of the study are to remove the effects of flow distribution during the test. According to the tests, if the tee is used before the orifice meter, there was not a difference in the straightener performance and this situation is independent on the straightener types [2].

The effects of different entrance flow velocity profiles on the quality of an orifice flow meter with and without flow conditioner were investigated as experimental by Quazzane et al. Two flow conditioners were studied as vaned plate, and NEL plate flow conditioner. In the scope of this study, radial velocity, swirl, and turbulence measurements were interviewed. Considering the test results, the occurred error due to the pipe fittings, cannot be ignored. Moreover, the efficiency of the vaned plate is lower than NEL conditioner.[3]

The effects of the different fractal straightener types on pressure drop after the fractal plates in the pipe were investigated as experimental by Aly et al. They manufactured an orifice of the Von Koch type. Two group straighteners were created such as increasing flow area, and decreasing flow area, which is shown in Figure 1.1 and Figure 1.2.

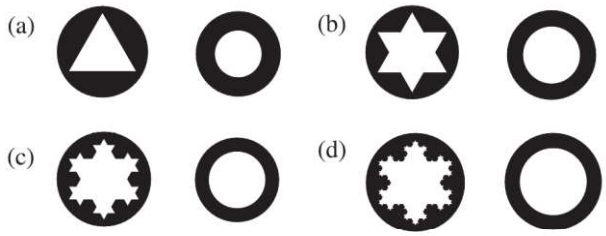

Figure 1.1 The different Generations of the Fractal Plates; (a) Base Design, (b) First Iteration Design, (c)The Seconds Iteration Design, (d) The Fourth Iteration Design

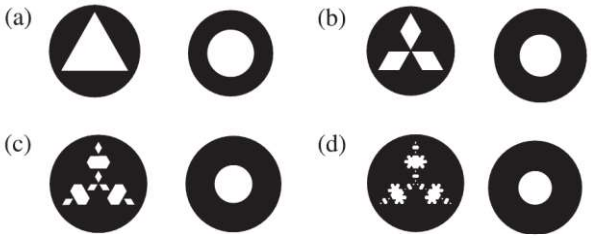

Figure 1.2 The Different Generations of Fractal Shaped; (a) Base Pattern, (b) The First Generation, (c) The Seconds Generation, (d) The Third Generation

During the tests, pressure values were measured from the different locations. The test results were compared in the scope of the pressure drop. The optimized sizing of Von Koch type air flow conditioner provides low pressure loss in the pipes [4].

In Brown and Griffith's study, a flow conditioner was added to an ultrasonic meter and the effects of it on the pressure loss were investigated as experimental. Totally, 31 straighteners, which have the same type, however, they consist of different hole sizes, different numbers of holes and different thicknesses, were created. One of them is shown in the following figure. According to the experimental results, for use with a 4-path ultrasonic meter, the measurement results with the new straightener are equivalent to the Laws type plate, but they accomplished it with less than half the pressure loss [5].

The effects of different porosities on the air straighteners in the pipe were investigated as experimental by Razali et al [6]. Considering the test results, when the porosity rate of the flow conditioner is increased, the pressure drop due to the air conditioner is decreased.

Three conditioners, which are a tube bundle, and two different perforated plates, are Akashi type and Laws type, were investigated as experimental with velocimetry and hot wire anemometry at high Reynolds numbers by Xiong et al. Velocity profiles,

turbulent fluctuations and Reynold stress were measured during the tests. According to the test results, the perforated plates have a higher efficiency than the tube bundle straightener. [7]

An experimental study was conducted to investigate the decay process of high swirling in a pipe and its effect on flow meter reading values by Laribi et al [8]. The Etoile, Tube bundle and Laws perforated plates were used during the tests. Laser Doppler Anemometer was selected to measure velocity and turbulence. The best values were observed by the Laws perforated plate for the velocity profile. Tube bundle type conditioner provided the best swirl angle. The writer suggests that the two different plates can be combined to observe the best solution.

1.1.2 Numerical Studies

The circle grid shape of fractal plate was studied by Pramiyanti et al. He aims to reduce the distortion due to the asymmetric profile by removing the swirl [9]. Therefore, fractal plane was created at three different thicknesses (1mm 3 mm, 6mm). The internal flow was solved via computational methods. The results of this investigation represent changes of the pressure recovery, velocity profile and velocity vectors for a variety of combinations of the orifice plate and disturbances [9]. The velocity values were compared between swirling flow without through the fractal plate and swirling flow through the fractal plate at the three same positions. 6 mm thickness fractal plate is suggested for the pipes [9]. The fractal plate is shown in Figure 1.3.

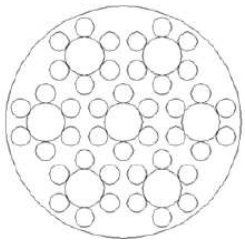

Figure 1.3 The Schematics of Fractal Plate [9]

Many different straighteners are designed and used in the ducting. International Organization for Standardization offers several straighteners to support better flow characteristics, like Zanker, Tube Bundle, etc [10].

The performance of an Etoile flow conditioner downstream of a vortex generator is reviewed, finding that the related model provides to smooth the abnormal flow field by Chen and Liu [11]. An octagonal star shaped improvement method is used in this study. A new straightener was designed, which has better performance than the Etoile air conditioner.

The different flow conditioners were investigated, and new straighteners are created to reduce dynamic loads for water flow in pipes by Zaryakin et al [12]. A perforated disc, a slot type, a duplex slot type, a linear circumferential, a plate-type and a sectoral flow conditioner are studied in the scope of the article and are shown in Figure 1.4.

Figure 1.4 The Different Conditioner Applications [12]

The computational method was selected as the solution method. Ansys Fluent was used as tool. The k-epsilon turbulence model was selected as turbulence model. The efficiency of all conditioners is compared in this study [12].

A flow straightener was added to International Fusion Materials Irradiation Facility (IFMIF) by Gordeev et al [13]. Two different types of conditioners were designed, and three different turbulence models, which is k-epsilon realizable, k-omega SST, and Reynolds Stress (RSM) turbulence models, were used in the simulations via Star CCM+. The used straighteners consist of honeycomb types as a rectangular shape. The simulation results with three different turbulence model are compared with experimental results. The RSM turbulence model provides quantitatively and qualitatively the most accurate pressure loss data and average velocity counter [13].

Moreover, the honeycomb type straighteners are insufficient for short axial distances [13].

The turbulent swirling flow through the Zanker plate was investigated at five different turbulence models in order to determine the most suitable turbulence models to model such air flow problems by Drainy et al. The smaller holes were designed near the plate edge in order to break down the swirl, which intensifies near the boundary. This increases the efficiency of the straightener. Moreover, the effects of conditioner thickness, plate hole sizes on the flow were investigated. The most important aim of this study determines the optimum straightener thickness. Pressure drop, tangential velocity and swirl angle values at four different flow rates were compared during all numerical simulations. The standard k-epsilon, the realizable k-epsilon, Reynolds stress, Large Eddy Simulations (LES), and Detached Eddy Simulation (DES) were used in the simulation. DES turbulence model yielded better agreement than other examined models [14]. Plate thickness was proved to be inversely proportional to the swirl angle and tangential velocity component [14].

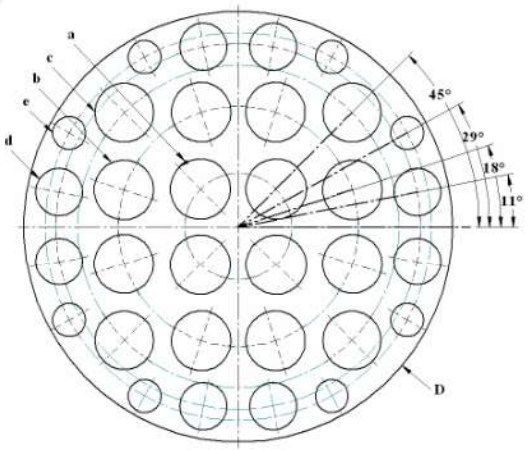

Figure 1.5 The Zanker Plate Schematics [14]

1.1.3 Experimental and Numerical Studies

Both numerical and experimental studies are conducted on Fi-fi monitor by Bilir [15]. Fi-fi monitor consists of the ducting. Three different flow conditioners, which are Zanker, Tube Bundle, Unique, are applied into the ducting at three different lengths (50mm, 100 mm, and 200mm). The numerical analysis was modeled via Star CCM+. The turbulent flow was modeled using the k-w SST turbulence model. Y+ was adjusted

between 30 and 300. Experimental studies are applied through 200 mm unique model at five different pressure values. After the completion of the experimental test and simulations were compared and one model is suggested for fi-fi monitor.

There are several straighteners' models like vortab, disturbance plate, tube types, etc. in Miller documents [16], which are shown in Figure 1.6.

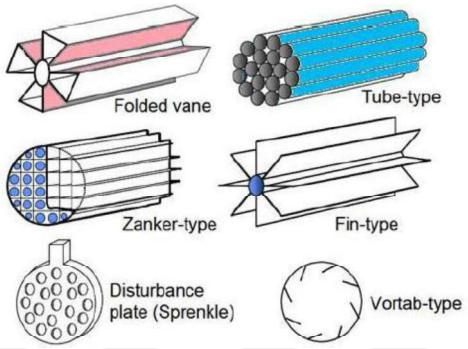

Figure 1.6 Some of The Air Flow Conditioners [16]

The use of straightener types or flow meter types was explained, and theoretical approaches were shared by Crabtree [17].

The flow straighteners were designed to prevent swirl creation in the flow. Although it has so many advantages in flow, there are several thoughts about velocity, swirl angle and turbulence measurements. Baker explained the evaluation methods.[18]

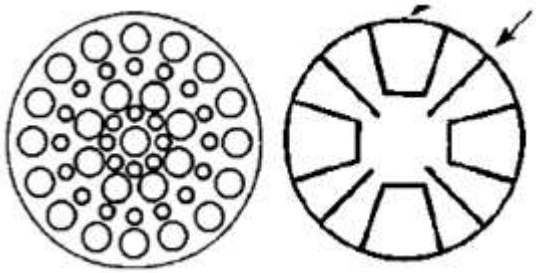

Figure 1.7 The Schematics of K-Lab and Vortab Type Straighteners [18]

Studies of Askari et al. [19] are conducted over the NEL Sperman and Mitsubishi flow conditioners. CFD model was developed and compared with experimental data. The velocity profile and the swirl results are presented COMSOL software. The k-epsilon turbulence model is used in the simulations. A new model was created and the thickness, position of holes and shape of the holes were modified. Then, all numerical results are compared, and one flow conditioner design is preferred.

Figure 1.8 NEL Spearman and Mitsubishi Flow Straighteners, respectively [19]

Another study was conducted by Bayazit et al [20]. The effect of laminar and turbulent flows properties, the thickness of straighteners on fluid properties and convective heat transfer is investigated in this study [20]. The square and staggered type flow straighteners are modeled, which are shown in Figure 1.9.

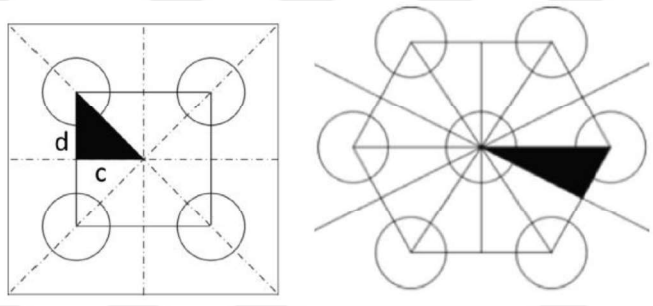

Figure 1.9 The Square and Staggered Flow Straighteners [20]

The simulation conditions are steady fluid flow, three dimensional and RANS equations are used via Ansys Fluent. Taken results are compared with experimental results. As a result, the most quality straightener model is found for this study [20].

Etoile, perforated plate, and tube bundle were installed an air compressor system, which was investigated pressure losses and turbulence intensity by Carpioglu and Ozahi both as numerical and as experimental [21]. According to the results, minimum pressure losses occur at the tube bundle. However, maximum pressure losses occur at the perforated plate during all Reynolds Numbers [21].

Creating a sufficient fractal plate was studied under the standard and non-standard flow conditions both as experimental and using simulation by Manshoor et al [22]. The fractal plates were created at the fourth iteration, which is shown in Figure 1.10.

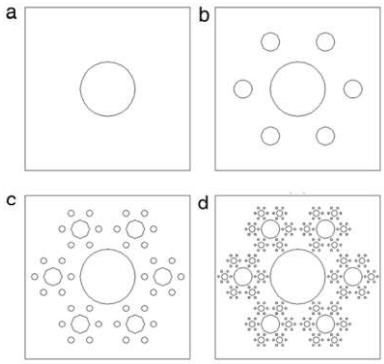

Figure 1.10 The Fractal Space Filling; (a) First Iteration, (b) The Seconds Iteration, (c) the Third Iteration, (d) The Fourth Iteration

Both two dimensions and three dimensions simulations were conducted. The k-epsilon turbulence model was selected by the writer. Then, simulation results were compared with experimental results. The results show that, the fractal plates can descent the distortion due to asymmetric velocity profile and also swirling flow on metering for high and low Reynold's Number [22].

Vaidya et al. [23] aim to understand the behavior of swirl flow in a pipe. Both numerical studies via Star CCM+ and experimental studies are conducted at two different swirl conditions. Honeycomb was selected as the flow conditioner. In the scope of this study, different simulation models were applied such as Direct Numerical Simulations (DNS) using time-dependent Navier Stokes equations, the implicit Crank Nicolson scheme, which is second order in time. The turbulent intensity and velocity contours were investigated, and the results are compared with the experimental results.

The different fractal plates, which consist of different porosities, were created 3-D program, and were manufactured by Lahadi et al. They conduct both numerical and experimental studies in order to define the effects of the changing porosity of the plates on pressure drop and turbulent intensity. The high porosity plate provides low turbulence intensity nearly downstream [24]. This fractal plate can be used for a combustion chamber according to the results of this study [24].

CHAPTER 2

FLOW DISTRIBUTION INVESTIGATION FOR THE DUCTING WITH EXPERIMENTAL METHODS

The helicopter cockpit air distribution ducting is produced in the scope of the test. The test ducting and routing are the same ducting found on the helicopter. Air ducting consists of twenty-six ducts. Materials of its are composite and flex. There are totally the ten air outlets. Five air outlets are located on the left side of the air distribution ducting. The others are located on the ride side of the air distribution ducting. Left-side air outlets and right-side air outlets are identical to each other. The ducting and routing are shown in Figure 2.1.

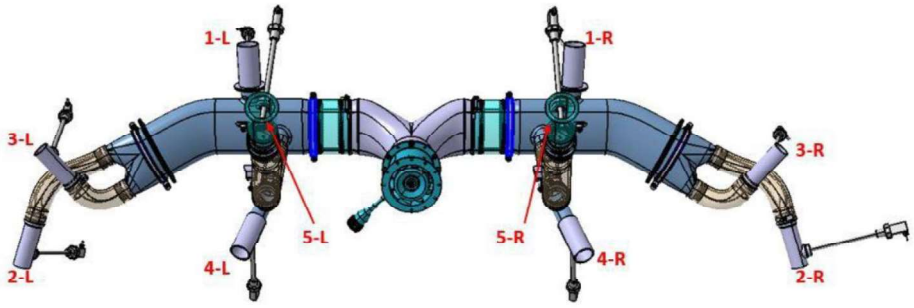

Figure 2.1 The Air Distribution Ducting

One fan is utilized in order to drive air from the helicopter inside to the air distribution ducting. The related fan includes two sections such as rotor and stator. The rotor zone is a moving zone and provides force to air. When the fan is powered by an electrical power supply, a negative pressure is created on the fan inlet section and air, in the helicopter cockpit zone, is derived to the rotor blades. The rotor section of the fan has ten blades. When the rotor blades are moved, they apply a rotational force to the air. After the rotor blades, the air takes a swirl form. Therefore, a stator zone requires in the fan. The stator zone has no motion since the aim of the zone is to regulate air flow, coming from the rotational zone. It includes the seventeen equivalent blades. The fan zones and blades are shown in Figure 2.2.

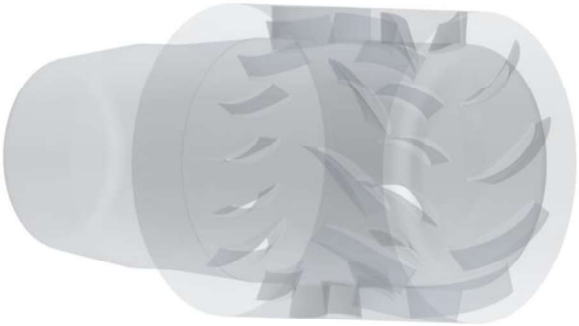

Figure 2.2 The Used Fan on The Air Distribution Ducting

In the scope of the test, air velocity measurements are required from each air outlet. Therefore, the ten Schmidt technology air velocity sensors are used to measure. It provides the voltage value during the measurement time range. Air velocity value is calculated from the voltage values. The related formulations are provided by the sensor company, are given in the following.

$$A = \frac{\pi}{4} \cdot D^2 \tag{2.1}$$

$$V_A = PF \cdot V_C \tag{2.2}$$

Profile factor (PF) is defined depending on the diameter of the measuring pipe for pipes with circular cross-sections by the sensor supplier [25]. The defined values are given in the following table.

Table 2.1 The Lists Profile Factor for Standard Pipe Diameter

Inner Diameter of Pipe (mm)	Profile Factor
51	0.772
70	0.786
100	0.804
125	0.812
150	0.817
206	0.825
260	0.835

Each of the ten flow sensors is located at each air outlet within a duct. Sensor duct

diameters are the same, and their lengths are the minimum required value, which is defined by the flow sensor company.

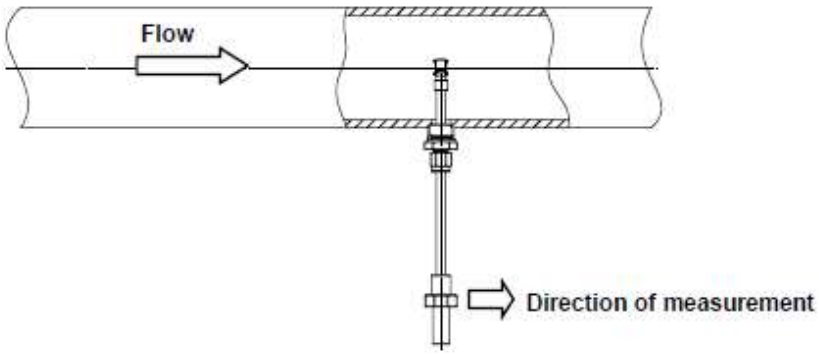

Figure 2.3 The Sensor Installation in The Air Ducting

The velocity measurement point is set to the center of the ducting. Various tests are performed to determine the center of the relevant ducting. The tests are applied under the same air mass flow rate. During the test, the sensor probe is submerged in the duct step by step. End of each test, test air velocity is calculated depending on the amount of immersion. The velocity distribution formed in the duct is deduced as in Figure 2.4.

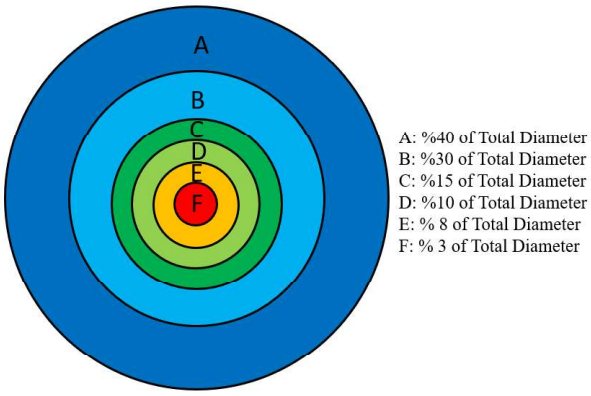

Figure 2.4 The Velocity Distribution in The Pipe in order to Install Flow Sensor

Both the fan and the flow sensors are powered by an electrical power supply. They operated 28 V DC electrical power. It provides a minimum 100 Ampere current capacity.

The three-laboratory test are conducted at three different rotational fan speeds, that's 6250 rpm, 9250 rpm and 12550 rpm. Calculated air velocity for each air outlet at each rotational fan speed is given in Figure 2.5, Figure 2.6, and Figure 2.7, respectively.

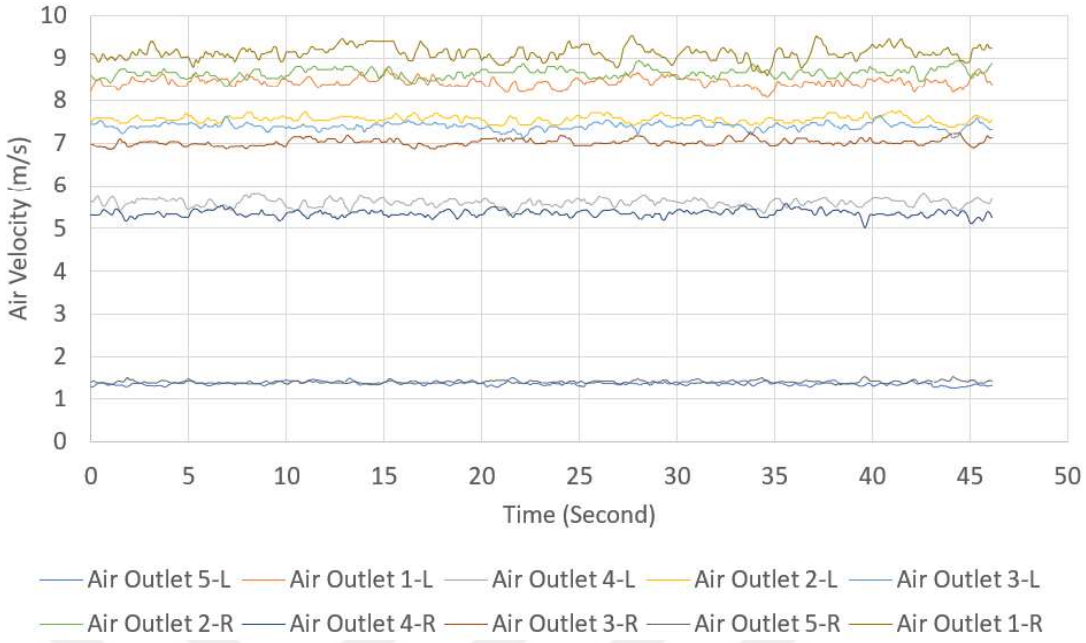

Figure 2.5 Air Velocity Measurement Values at 6250 rpm

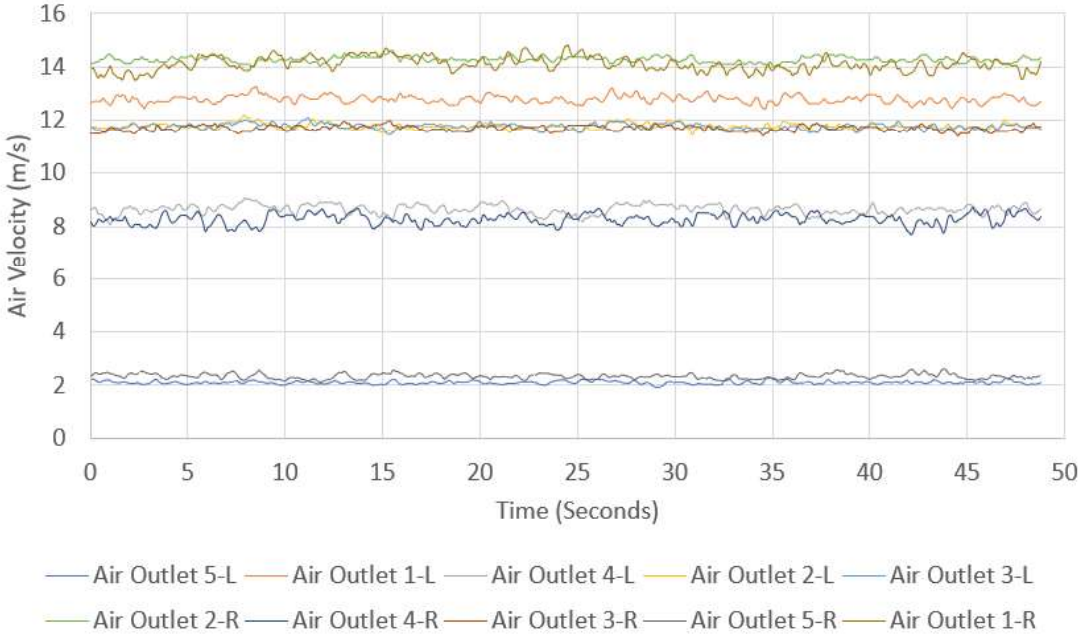

Figure 2.6 Air Velocity Measurement Values at 9250 rpm

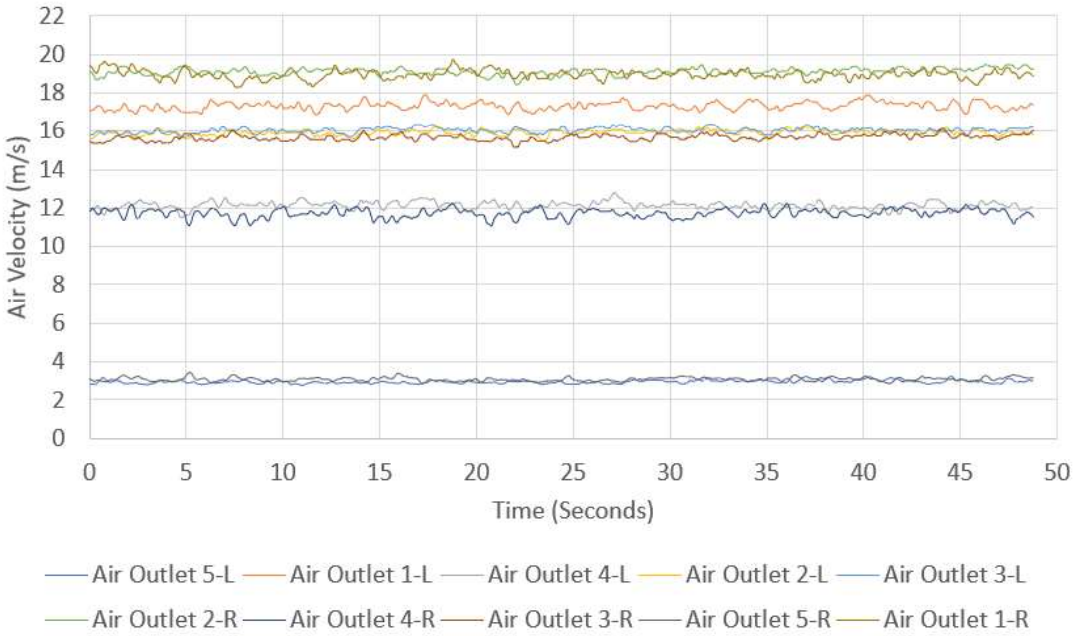

Figure 2.7 Air Velocity Measurements at 12250 rpm

CHAPTER 3

COMPUTATIONAL METHODOLOGY

3.1 Reynolds Averaged Naiver Stokes (RANS)

Reynolds Averaged Navier Stokes (RANS) is a computational method. The equations are used to model turbulent flow. Models of RANS turbulence is based on empirical observations.

For a stationary, incompressible flow of Newtonian fluid, these equations can be written in Einstein notation as:

$$\frac{\partial}{\partial t}\int_V Q\, dV + \oint_S (F \cdot n)\, dS - \oint_S (F_v \cdot n)\, dS = \int_V s_T\, dV \tag{3.1}$$

Where,

$$Q = \left\{\underline{\rho}\ \underline{\rho}\ \underline{u}_1\ \underline{\rho}\ \underline{u}_2\ \underline{\rho}\ \underline{u}_3\ \underline{\rho}\ \underline{e}_0 + \left(\underline{\rho' e'} + k\right)\right\},$$

$$\begin{aligned} F_j = \Big\{ & \underline{\rho}\ \underline{u}_j + \underline{\rho' u'_j}\ \underline{\rho}\ \underline{u}_1 \underline{u}_j + \underline{p}\delta_{1j} + \underline{u}_1\ \underline{\rho' u'_j} \\ & + \underline{\rho' u'_1}\ \underline{u}_j\ \underline{\rho}\ \underline{u}_2 \underline{u}_j + \underline{p}\delta_{2j} \\ & + \underline{u}_2\ \underline{\rho' u'_j} + \underline{\rho' u'_2}\ \underline{u}_j\ \underline{\rho}\ \underline{u}_3 \underline{u}_j \\ & + \underline{p}\delta_{3j} + \underline{u}_3\ \underline{\rho' u'_j} \\ & + \underline{\rho' u'_3}\ \underline{u}_j\ \underline{\rho}\ \underline{h}_0 \underline{u}_j + \underline{e}_0\ \underline{\rho' u'_j} \\ & + \left(\underline{\rho' e'} + k\right)\ \underline{u}_j \Big\} \end{aligned} \tag{3.2}$$

And,

$$F_{vj} = \left\{0\ \underline{\tau}_{1j} - \tau^T_{1j}\ \underline{\tau}_{2j} - \tau^T_{2j}\ \underline{\tau}_{3j} - \tau^T_{3j}\ \underline{u}_i \underline{\tau}_{ij} - \underline{q}_j + \Theta^T_j\right\} \tag{3.3}$$

The left side of the equation describes changes in the mean momentum of the fluid element due to the instability in the mean flow and the convection by the mean flow [26]. This change is balanced by the mean body force, the isentropic stress owing to the mean pressure field, the viscous stresses, generally referred to as Reynolds stress [26]. The related term requires additional modeling to close the RANS equation to solve.

The flow quantities are divided into time-averaged and fluctuating parts with this methodology. The related equation includes velocity variable (u), time mean averaged component ($\underline{Ui}$) and fluctuating component ($\dot{U}\imath$), is shown:

$$U_i = \underline{Ui} + \dot{U}\imath \tag{3.4}$$

The same formulations are defined for pressure and other parameters.

The averaging process may be thought of as time-averaging for steady-state situations and ensemble averaging for repeatable transient situations. Inserting the decomposed solution variables into the Navier-Stokes equations results in equations for the mean quantities [27].

3.2 The K-Omega SST Turbulence Model

Since the Simcenter StarCCM+ consists of the two main types of turbulence models such as RANS and solve for large scales of turbulence and model small scale motion.

K-Omega mode provides improved performance for boundary layers under adverse pressure gradients. On the other hand, the biggest disadvantage of the K-Omega model, in its original form, is that boundary layer computations are sensitive to the values of the free-stream.

The K-Omega turbulence model consists of the two-equation model to solve transport equations for the turbulent kinetic energy k and the specific dissipation rate (ω).

The turbulent kinetic energy (k) is given as [28]:

$$k = \frac{3}{2} \cdot (UI)^2 \tag{3.5}$$

Where U is the mean flow velocity, and I is the turbulence intensity.

The specific turbulent dissipation rate (ω) is defined as the following formulas:

$$\omega = C_{\varphi}^{\frac{3}{4}} \cdot \frac{k^{\frac{1}{2}}}{l} \tag{3.6}$$

where C_φ is the turbulence model constant which usually takes the value 0.09, k is the turbulent energy, l is the turbulent length scale.

3.3 Wall Treatment

Walls are modeled during many of the simulation studies. Therefore, turbulence and flow parameters near the wall boundary layer should be predicted accurately.

In the K-Omega models, the wall treatment performs three important functions such as reference velocity (U^*), turbulent production (G_k), specific dissipation (ω) [27].

For the whole y+ values, a blending function "g" is defined in terms of the wall distance Reynolds number [27]:

$$g = exp\,(-\frac{Re_y}{11} \tag{3.7}$$

$$Re_y = \sqrt{k} \cdot \frac{y}{v} \tag{3.8}$$

The equation (9) is a wall distance based Reynolds number.

The reference velocity is not used during the low y+ simulation corresponding to the Star-CCM+. U^* formulation is shown in below:

$$U^* = \sqrt{\frac{gvu}{y} + (1-g)\beta^{*\frac{1}{2}}k} \tag{3.9}$$

Wall cell production (G_k) is calculated for low y+ as:

$$G_k = \mu_t \cdot S^2 \tag{3.10}$$

3.4 Multiple Rotating Reference Frame (MRF) Method

All air conditioning systems include a minimum of a fan. The air has derived a fan through air distribution ducting to the cockpit zone. One of the important points in the

air distribution ducting is to provide the same amount of air flow from the air outlets. Initially, the air distribution routing is created depending on the rotorcraft space envelopes. Then, computational fluid dynamics calculations are conducted since the CFD method has low cost and quick results.

The fans can generally be modeled at two different methods, such as defining pressure difference, multiple rotating reference frames. In this study, multiple rotating reference frame is used to model the related fan since this method provides a robust result, in which the fan geometry is rotated in the related zone.

The MRF approach is a baseline for multiple zones according to many studies. It is a steady-state approximation in which individual cell zones can be assigned different rotational and/or translational speeds [29]. Air in the rotating zone is solved using the moving reference frame equations. If there is a stationary zone, the equations reduce for related simulation suctions. For the interfaces between zones of interest, a local reference frame is defined to provide the flow variables and calculate the flow value along the boundaries [29].

The mesh, which is filled, remains during the calculations. This is analogous to freezing the motion of the moving part in a specific position and observing the instantaneous flow field with the rotor in that position [30]. An example of an MRF application is a fan-rotating zone, which is shown in Figure 3.1.

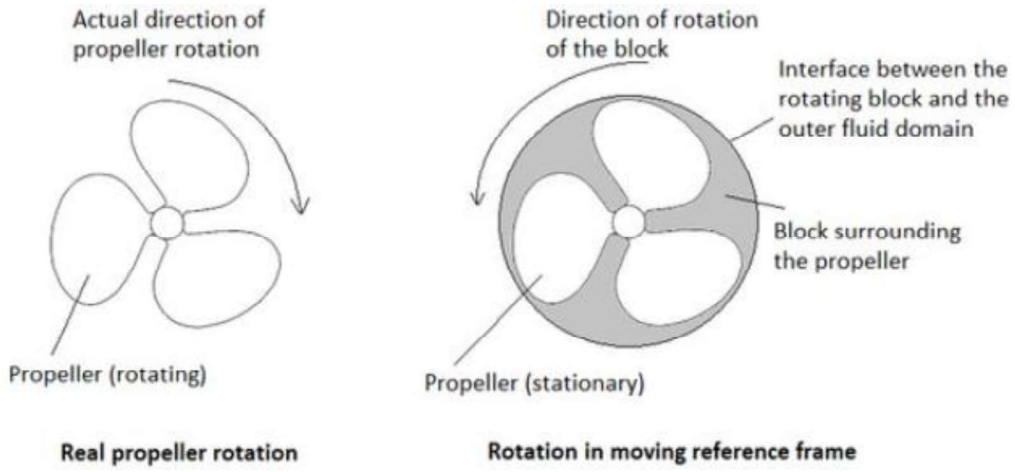

Figure 3.1 Working Principle of the Moving Reference Frame [30]

CHAPTER 4

FLOW DISTRIBUTION INVESTIGATION FOR THE DUCTING WITH COMPUTATIONAL METHODS

4.1 Description of Air Distribution Ducting

The related helicopter air cooling system has two distinguished air flow distribution ducting routing for the cabin and cockpit. Cockpit air flow distribution ducting is investigated and will be improved in the scope of the thesis.

Cockpit air outlets and ducting are identical for pilot/copilot zones. Air distribution ducting totally includes five air outlets for each pilot and co-pilot zones. An air outlet is located for each forward windshield, side windshield and low windshield. The other two air outlets are located for the pilot/co-pilot up and low body. Windshield air outlets are not adjustable type since there is used to remove demist on the windshield. The pilot/co-pilot up-body air outlet is designed as adjustable to provide a comfortable zone pilot and copilot. Another air flow outlet is directed to the pilot/co-pilot low body. Therefore, low-body air outlet is designed as non-adjustable. Helicopter cockpit air outlets are shown in Figure 4.1.

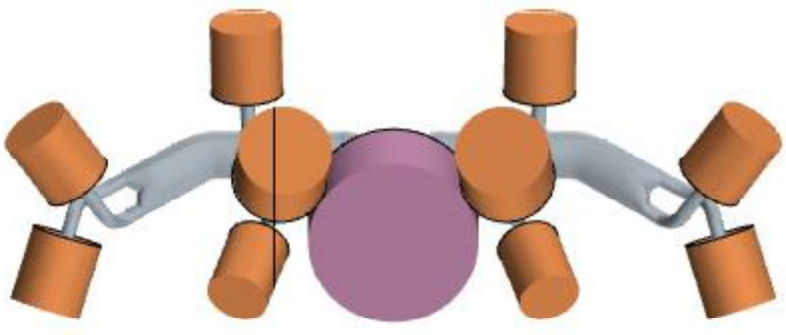

Figure 4.1 Air Distribution Ducting Air Outlets (Orange Colors)

Moreover, a fan is located on the helicopter cockpit air inlet to provide fresh and warm air to the windshield and crew members. The related fan can be operated at three different rotational speeds by the crew.

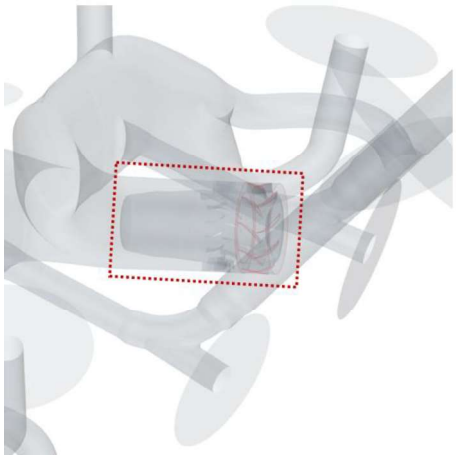

Figure 4.2 The Fan Locations on The Air Distribution Ducting

4.2 Development of Computational Fluid Dynamics Model

A physical air flow distribution between the left and right side of cockpit air ducting is investigated by using StarCCM+. A computational fluid dynamics model is created to simulate air mass flow rate distribution in ten air outlets and to compare each mass flow rate value on left and right-side air outlets.

In this simulation, the ducting model is created as unique in order to simulate the fan swirl effect on the air flow distribution between left and right-side air ducting, although left and right-side air distribution ducting is symmetric.

The gaspers of cockpit air outlets are designed as especially for the related helicopter. The five gaspers are different from each other. However, the gaspers of the left and ride side air outlet are identical. Additionally, to reduce the amount of mesh, simplify the simulation model, to reduce computational cost, cylindrical air outlets are used instead of complex air outlets. Simplify model is demonstrated by You et all [31].

Moreover, cylindrical air zones are added for both air inlet and air outlets to simulate the existing case. The air is vacuumed in the space by using a fan. On the other hand, the air is discharged to atmospheric region through air outlets. The diameter of the cylindrical is created five times of related air outlet ducting. This methodology is taken from “ANSI/AMCA210-07/ASHRAE 51-07 standard” [32]. The length of the cylindrical zone is identical on all air outlets (orange colour) and air inlet (magenta colour). It is defined to prevent reverse flow in the air outlet zone. The simulation

model is shown in Figure 4.3.

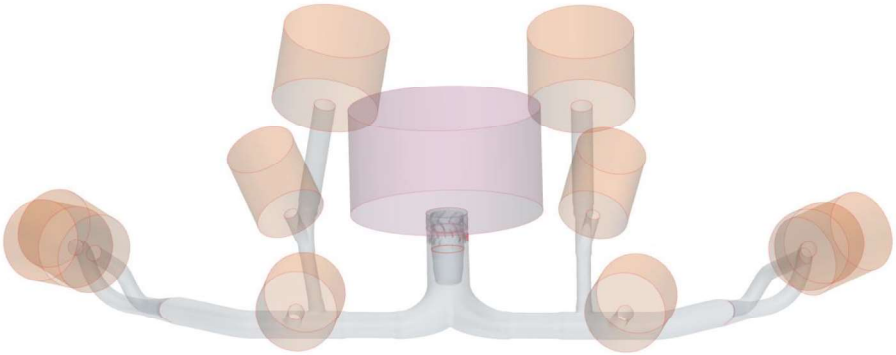

Figure 4.3 The Simulation Model

The air flow distribution between the left and right-side cockpit air outlets is important since imbalanced air flow from the air outlet affects the flow pattern in the cockpit zone. The importance of flow patterns in the helicopter cabin zone is investigated in Sahin study's [33]. Additionally, imbalance air flow from the air outlet affects defogging performance especially on the helicopter forward windshields. Some helicopters and aircraft are utilized the hot or fresh air derived from the fans.

Some assumptions are made in related study to focus fan swirl effect on the air flow distribution in the ducting. The temperature increases of the air due to the fan are not added to the simulations. Heat transfer during air distribution, between the outside of ducting and ducting outside surface, between ducting and air flow on the inside, is not calculated in this simulation. In this study, the main focus is to investigate the shape of ducting and the fan swirl effect on air flow distribution. Additionally, the surface roughness of composite ducting is assumed as negligible since left and right cockpit air ducting is symmetric and pressure drop is not investigated in this study.

Table 4.1 Applied Boundary Conditions

Boundary Definition	Boundary Type	Boundary Condition Value
Air Inlet	Stagnation Inlet	Pstatic_gage=0
Fan Rotor Zone	Moving Rotational Reference Frame (rpm)	Varied according to different cases
Fan Stator Zone	Wall	Uwall=0
Air Ducting	Wall	Uwall=0
Air Outlet	Pressure Outlet	Pstatic_gage=0

The Kw-SST model is preferred since the swirl effect is important in the scope of this study. Details of the related turbulence model are given in [34, 35]. Moreover, the k-omega SST turbulence model has been used in different studies such as [14, 16].

4.3 Mesh Independence Study

To investigate the air mass flow distribution in air distribution ducting, firstly a mesh independent solution must be obtained. In this study, polyhedral type mesh is used to fill volume and surface re-mesher is selected for the surface.

Three different mesh studies are conducted in the helicopter air distribution ducting. Base size, target surface size and minimum surface size are the main parameters to control surfaces and volume meshes. In this study, surface growth rate, number of layers, prism layer near wall thickness, prism layer total thickness and volume growth rate are kept the same for three mesh studies. Related parameter values are shown in Table 4.2.

Table 4.2 Defined Mesh Specifications and Their Values

Mesh Specifications	Mesh #1	Mesh #2	Mesh #3
Base Size [mm]	50	40	30
Target Surface Size [mm]	12	8	4
Minimum Surface Size [mm]	1.44	1.44	1.44
Surface Growth Rate	1.15	1.15	1.15
Number of Layers	25	25	25
Prism Layer Near Wall Thickness [mm]	1.2E-3	1.2E-3	1.2E-3
Prism Layer Total Thickness [mm]	4.0E-1	4.0E-1	4.0E-1
Volume Growth Rate	1.15	1.15	1.15

Moreover, specific surface controls are added to observe the best solution, which is the rotor & stator blades near the wall, leading & trailing edge of blades, stator zone surface, rotating zone, inlet, and outlet zone walls. Controlled surfaces are shown in Figure 4.4.

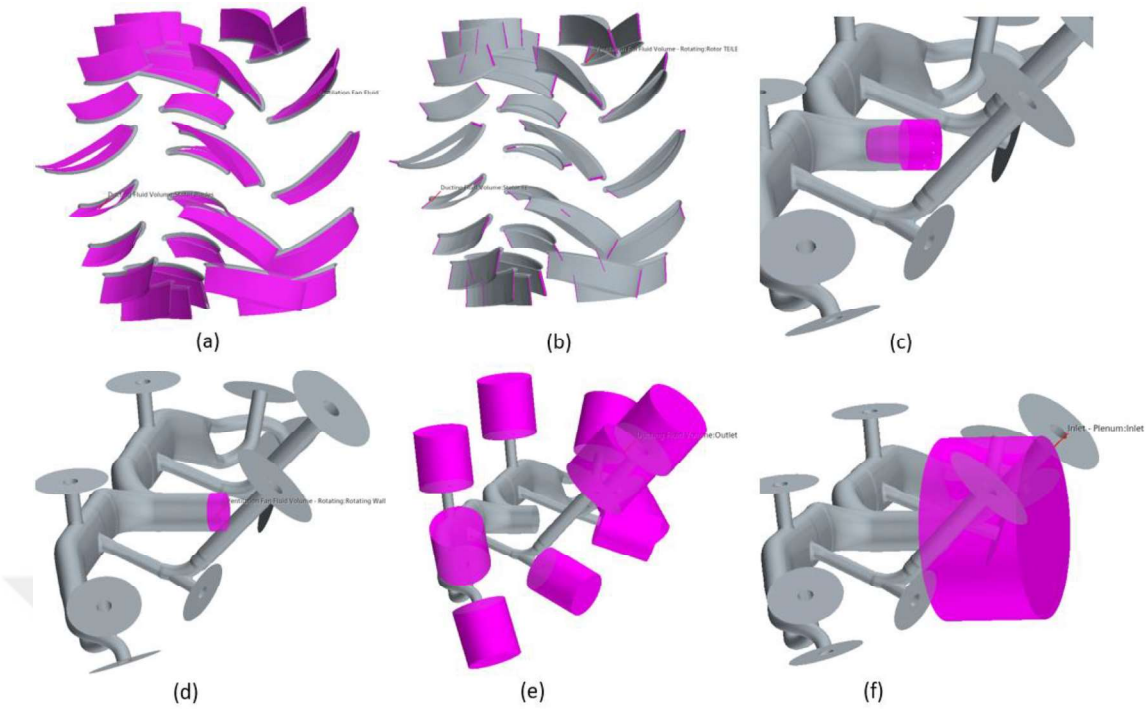

Figure 4.4 (a) Rotor and Stator Blades Near Walls, (b) Rotor and Stator Blades Leading and Trailing Edges, (c) Stator Zone Surface, (d) Rotor Zone Surface, (e) Air Outlets, (f) Air Inlet

Target surface and minimum surface size parameter values are changed for these surfaces, given values are shown in Table 4.3.

Table 4.3 The Given Mesh Parameters and Values for Controlled Surfaces

Surface Control Zone	Mesh Specifications	Mesh #1	Mesh #2	Mesh #3
Rotor & Stator Blades Near Wall	Target Surface Size [mm]	1.5	1.5	1.5
	Minimum Surface Size [mm]	2.25E-1	2.25E-1	2.25E-1
Rotor & Stator Blades Leading & Trailing Edges	Target Surface Size [mm]	1.5E-1	1.5E-1	1.5E-1
	Minimum Surface Size [mm]	7.5E-2	7.5E-2	7.5E-2
Stator Zone Surface	Target Surface Size [mm]	8	8	8
	Minimum Surface Size [mm]	1.44	1.44	1.44
Rotor Zone Surface	Target Surface Size [mm]	8	8	8
	Minimum Surface Size [mm]	1.44	1.44	1.44
Inlet Zone Surface	Target Surface Size [mm]	7	5	3
	Minimum Surface Size [mm]	1.44	1.44	1.44
Outlet Zones	Target Surface Size [mm]	8	4	4

Surface	Minimum Surface Size [mm]	1.44	1.44	1.44

The first layer thickness and total thickness are adjusted to observe y+ as 1. At all mesh studies and CFD models are used as same values after the y+ value is found as 1. Y+ values of rotating and non-rotating zones are shown as histograms in the following figures.

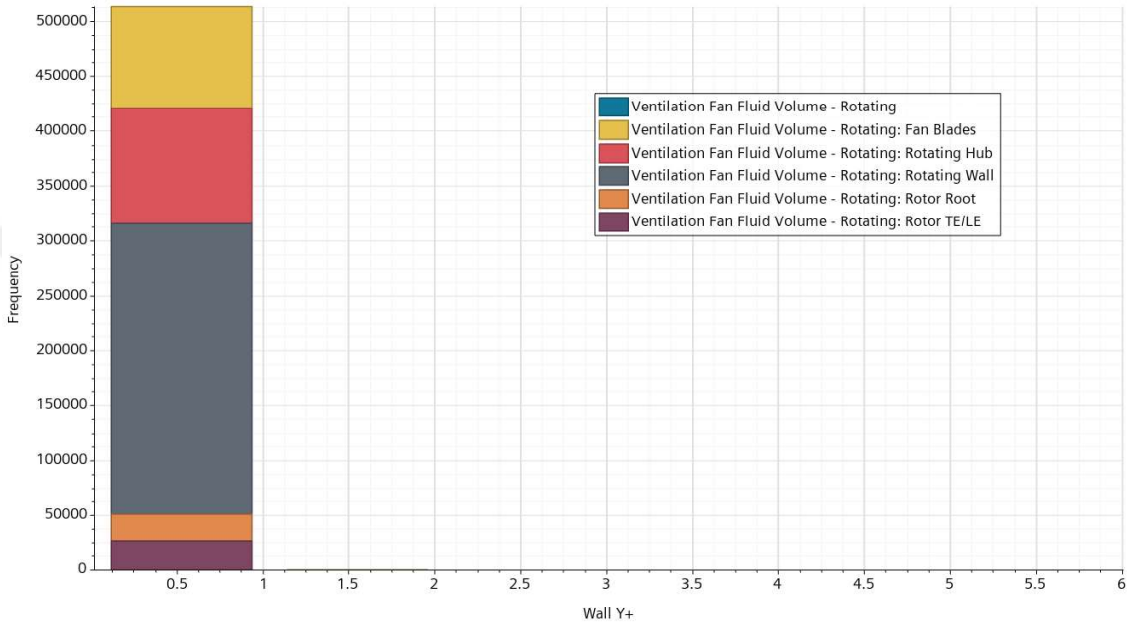

Figure 4.5 Rotating Zone Surfaces Y+ Values

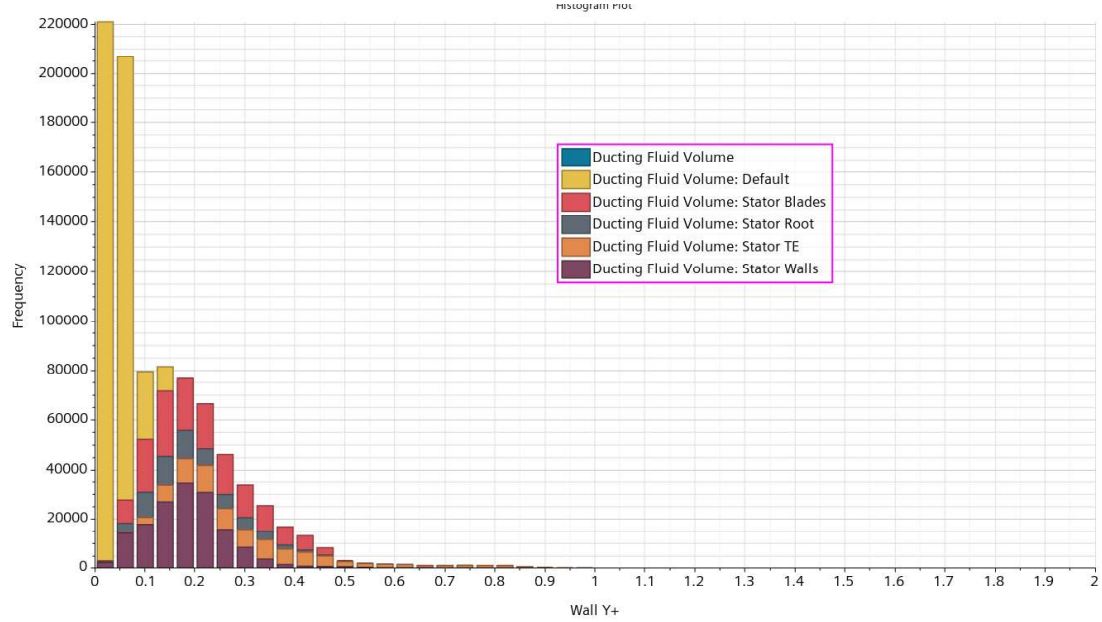

Figure 4.6 Non-Rotating Surfaces Y+ Values

The performance of numerical calculations is affected by mesh quality, therefore

shall be controlled to provide the best solution for calculations. The performance of mesh is evaluated on the four different parameters such as face validity, cell quality, volume change and cell skewness angle.

“The face validity is an area-weighted measure of the correctness of the face normal relative to their attached cell centroid. Values of below 0.5 signify a negative volume cell. A face validity of 1.0 means that all face normal are correctly pointing away from the cell centroid.” [27]

The cell quality metric algorithm is based on a hybrid of the Gauss and least-squares methods for cell gradient calculation methods [27]. A cell with a quality of 1.0 is considered perfect. A degenerate cell has a cell quality approaching zero. Cells with a face quality less than 1.0E-5 are considered bad [27].

The volume change metric describes the ratio of the volume of a cell to that of its largest neighbor [27]. A value of 1.0 indicates that the cell has a volume equal to or higher than its neighbors. Cells with a volume change of 0.01 or lower are considered bad cells [27].

This skewness measure is designed to reflect whether the cells on either side of a face are formed in such a way as to permit diffusion of quantities without these quantities becoming unbounded [27]. Cells with a skewness angle greater than 85˚ are considered bad cells.

Face validity, cell quality, volume change and cell skewness angle values of rotating and non-rotating zones are given for each mesh study in Table 4.4. Additionally, mesh quality details of all CFD zones are added to Appendix A, Appendix B and Appendix C for each mesh model.

Table 4.4 The Mesh Performance Values for The Different Meshes

Mesh Quality Parameters	Mesh #1	Mesh #2	Mesh #3
Minimum Face Validity	0.81	0.88	0.86
Minimum Volume Change	4.1E-05	2.44E-05	1.9E-05
Cell Quality	1.1E-05	3.2E-04	3.8E-04
Cell Skewness Angle	84	78	60

Total amount of volume mesh is given for each mesh studies in Table 4.5.

Table 4.5 Total Amount of Volume Mesh for Three Meshes

Amount of Mesh	Mesh #1	Mesh #2	Mesh #3
Volume Meshes	21E+06	25E+06	29E+06

The mesh study results of the fan zones, which are rotating and non-rotating zone, are shown in Figure 4.7 and Figure 4.8.

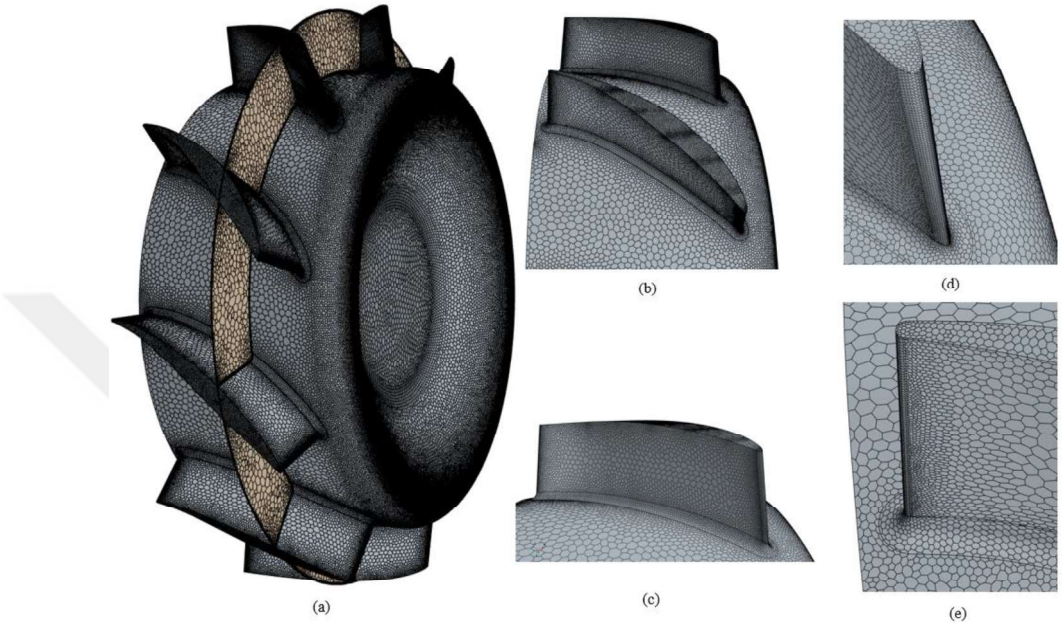

Figure 4.7 (a) Rotor Zone Volume and Surface Meshes (b) Rotor Blades Meshes (c) Near Wall of Rotor Blade Surface Mesh (d) Rotor Blade Leading Edge Surface Mesh (e) Rotor Blade Trailing Edge Surface Mesh

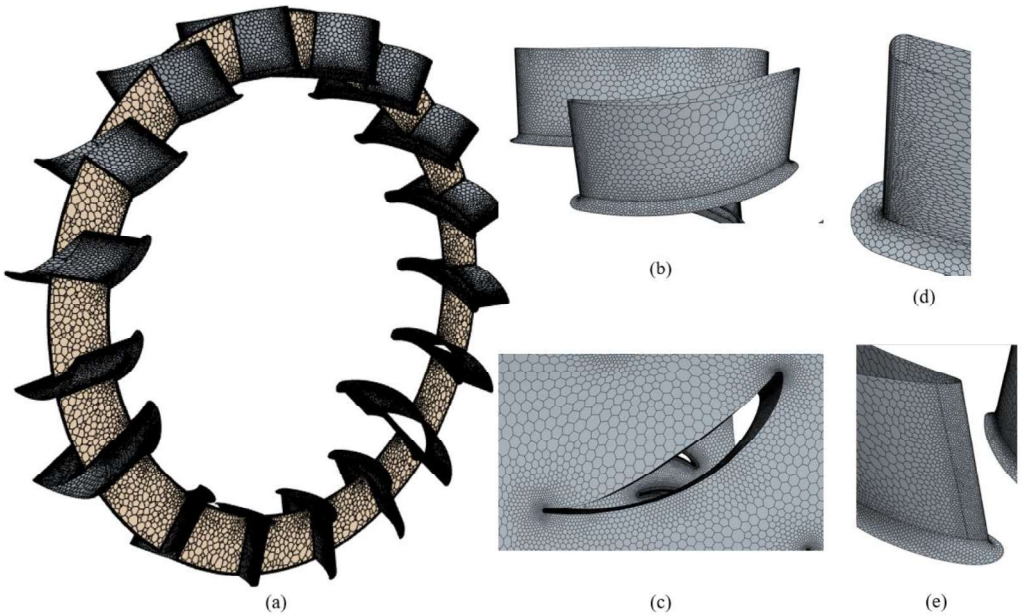

Figure 4.8 (a) Stator Zone Surface and Volume Mesh (b) Stator Balade Near Wall Surface Mesh (c) Upside Near Wall Stator Surface Mesh (d) Stator Blade Trailing Edge Surface Mesh (e) Stator Blade Leading Edge Surface Mesh

Three mesh studies are conducted at 12250 rotational fan speed. After the completion of the simulations, calculated air velocity values from each air outlet are compared with the measurement velocity value as experimental.

Considering the simulation results, the calculated air velocity value of Mesh #2 and Mesh #3 is very close with together. Moreover, these results are near the measured air velocity value. However, the difference between Mesh #1 simulation result and measured air velocity values as experimental is above 5 m/s. That's why and to reduce simulation running time and to descent simulation cost, Mesh #2 is taken as baseline mesh properties. The related results and air velocity comparison of each study and experimental results are given in Table 4.6.

Table 4.6 The Air Velocity Comparison of The Mesh Studies and Measured Values

Measured/ Calculated Air Outlets	Mesh #1 Simulation Air Velocity (m/s)	Mesh #2 Simulation Air Velocity (m/s)	Mesh #3 Simulation Air Velocity (m/s)	Measured Air Velocity (m/s)
1-L	15.8	17.4	16.6	17
1-R	20.8	19.3	19.2	19
2-L	14.8	15.1	15.4	15.6
2-R	14	14.5	16.7	18.2
3-L	17.2	15.1	15.5	15.6
3-R	13	13.3	13.9	15.1
4-L	15	14	13.4	11.5
4-R	13.1	12.4	11.7	11.8
5-L	7.5	7	6.6	3
5-R	5.4	3.6	3.4	3.1

4.4 Flow Distribution Investigation of the Located Air Routing on A Rotorcraft

In this chapter, flow distribution is investigated in the existing air distribution ducting using defined mesh properties (Mesh#2) at three different rotational fan speeds, such as 6250 rpm, 9250 rpm and 12250 rpm. Additionally, CFD results are compared with experimental results.

Point grids are created on the StarCCM+ Derived Part Section to monitor air velocity on the air outlets. CFD results are shown with point grids, which represent velocity (m/s), for each air outlet at three different rotational speeds, respectively.

Table 4.7 Air Velocity Distribution on the Each Air Outlet for 12250 rpm

Air Outlets	Left Side Velocity Grids	Right Side Velocity Grids
1	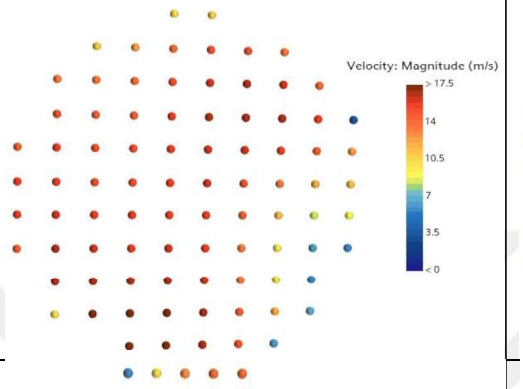	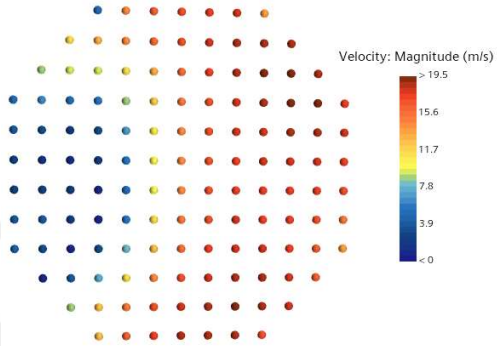
2	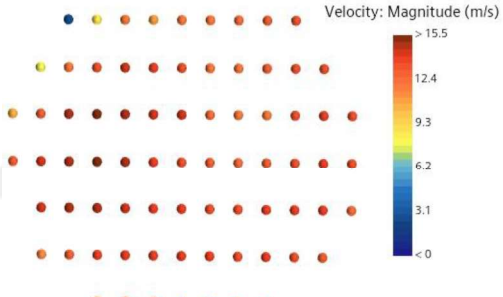	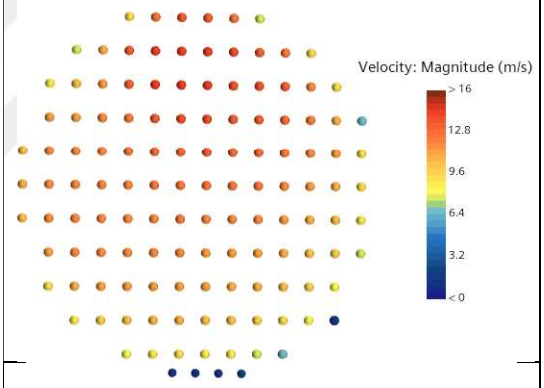
3	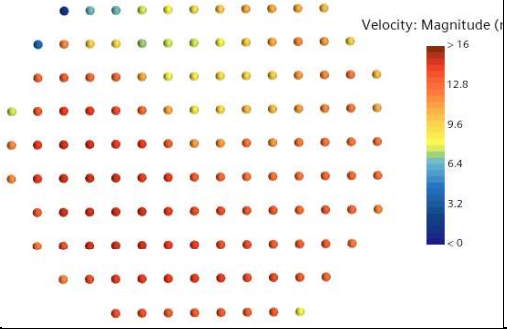	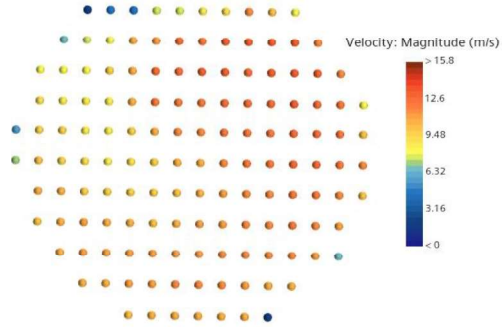

4	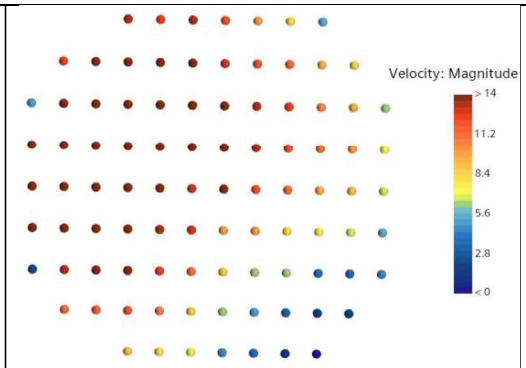	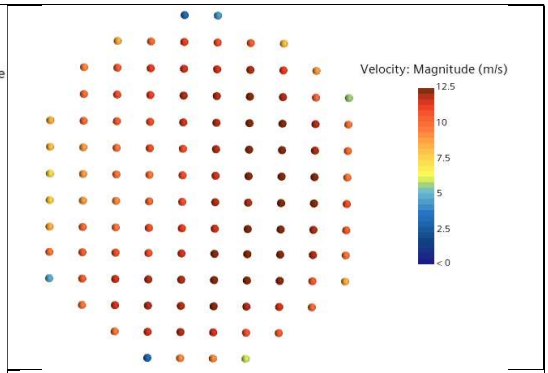
5	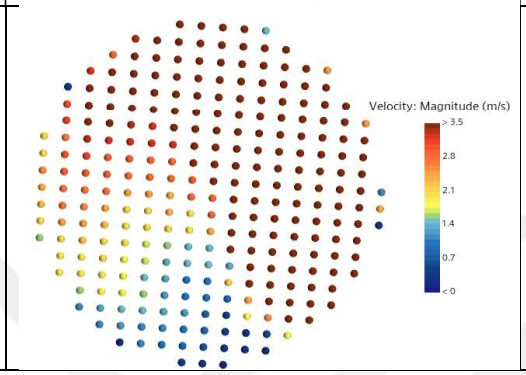	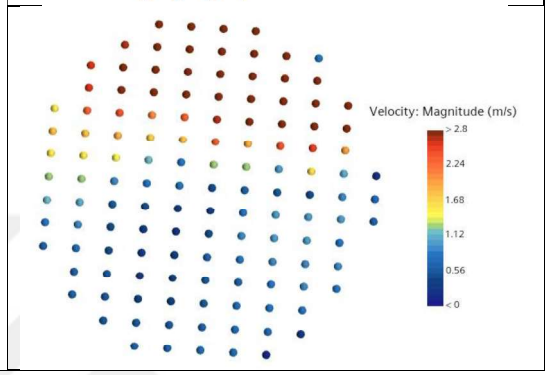

Table 4.8 Air Velocity Distribution on the Each Air Outlet for 9250 rpm

Air Outlets	**Left Side Velocity Grids**	**Right Side Velocity Grids**
1	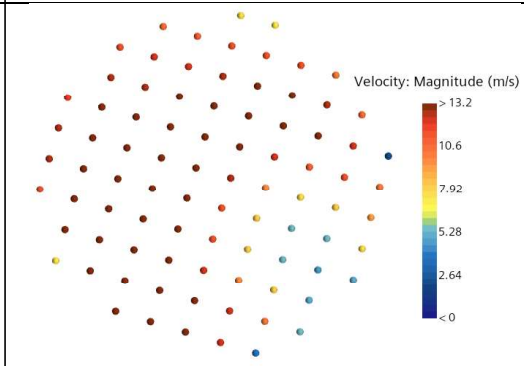	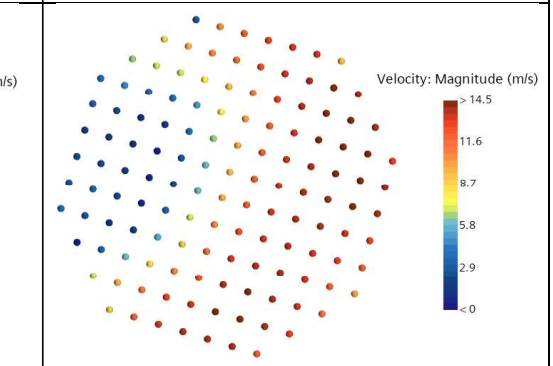
2	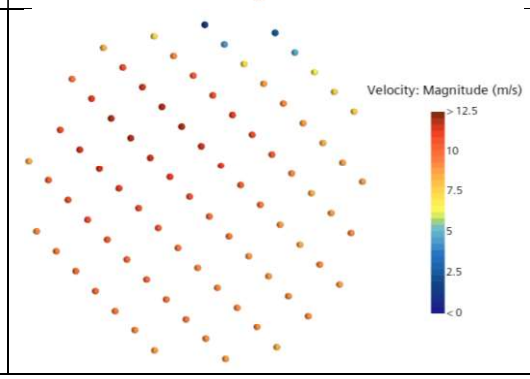	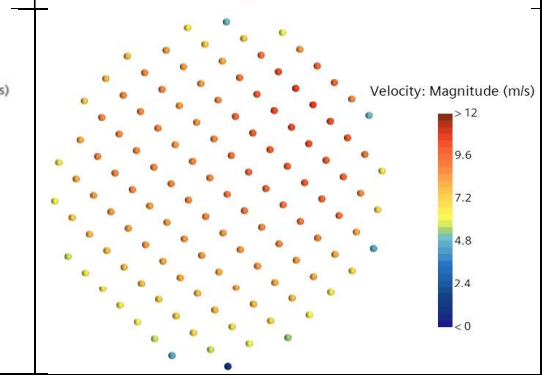

3	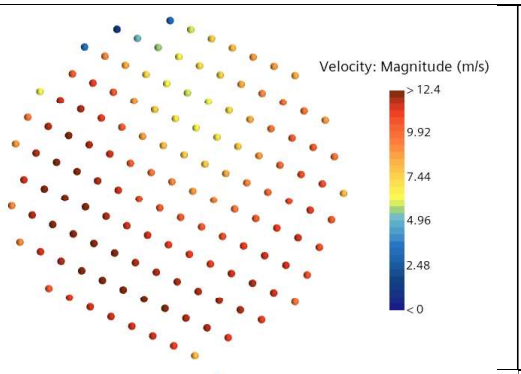	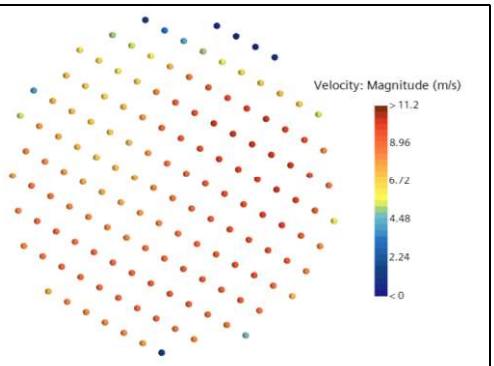
4	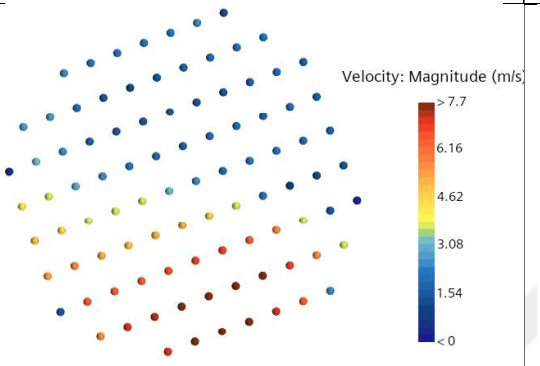	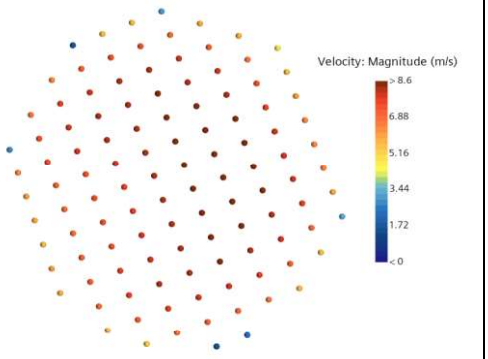
5	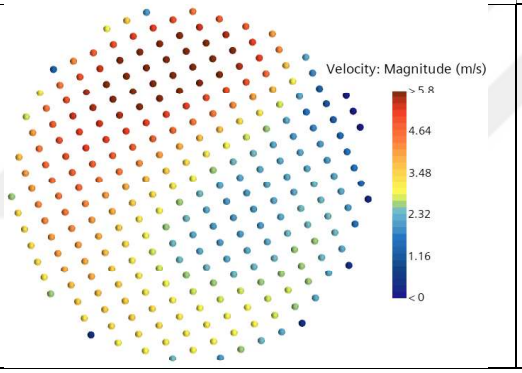	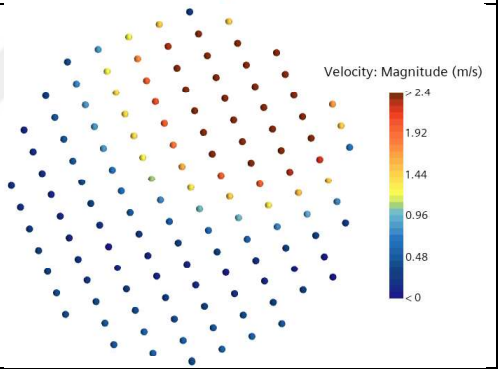

Table 4.9 Air Velocity Distribution on the Each Air Outlet for 6250 rpm

Air Outlets	Left Side Velocity Grids	Right Side Velocity Grids
1	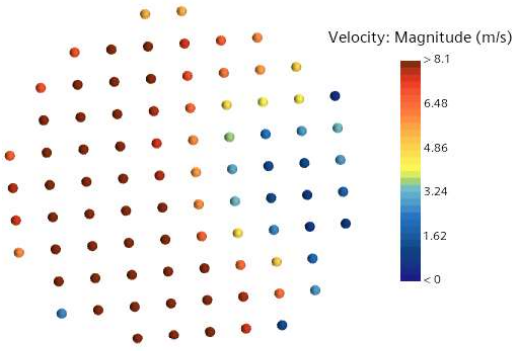	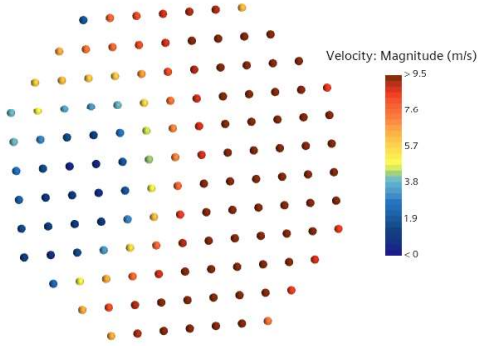

2	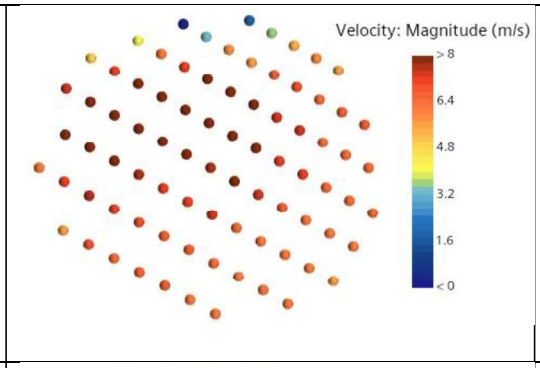	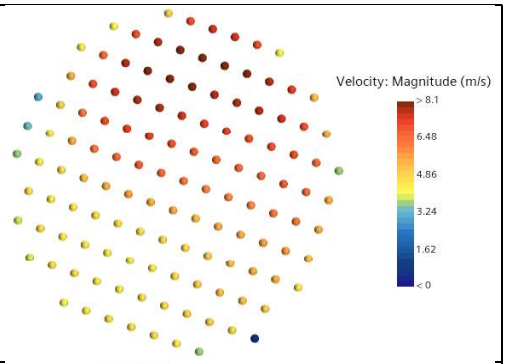
3	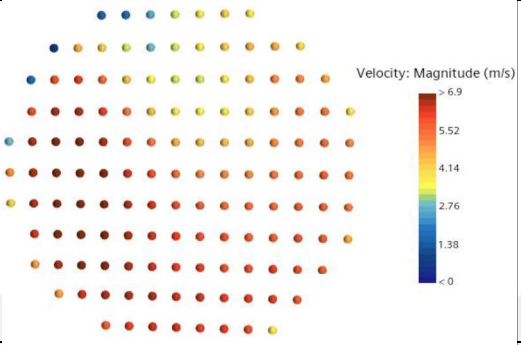	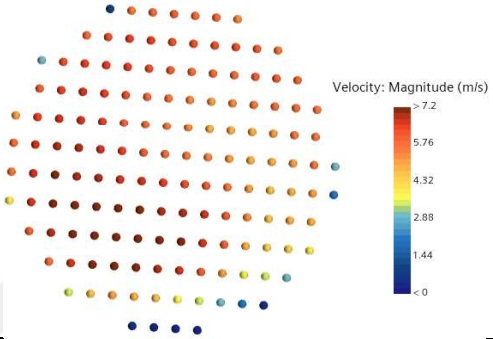
4	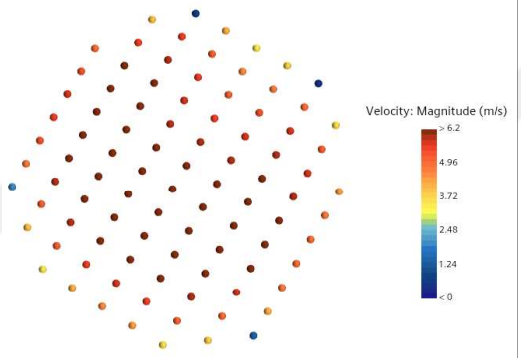	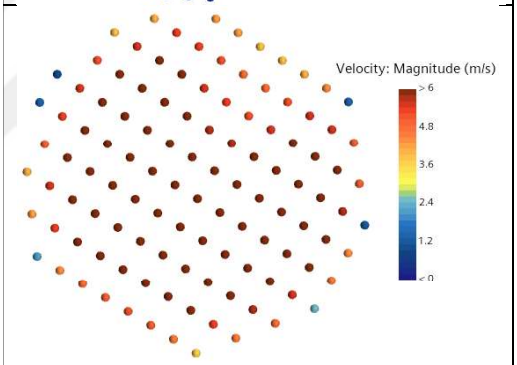
5	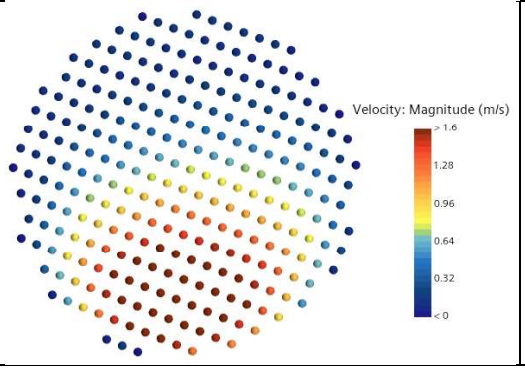	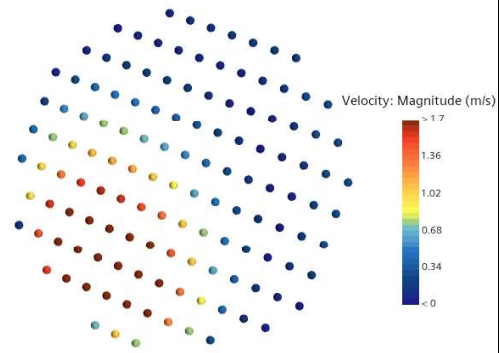

The total air inlet mass flow rate and total air outlet mass flow rate are compared to ensure that the correctness of the computational results. The related values are monitored, some of them are shown in Figure 4.9 and Figure 4.10, and others are given in Table 4.10.

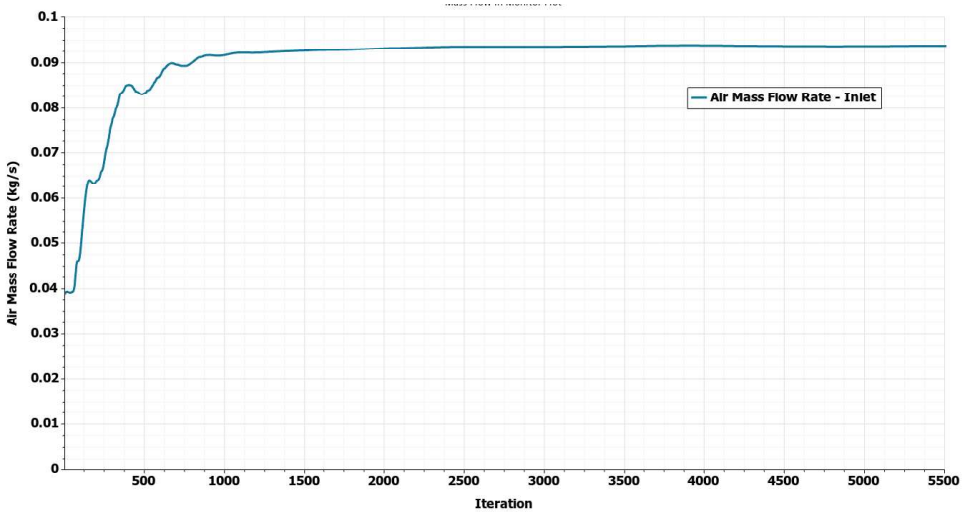

Figure 4.9 Air Inlet Mass Flow Rate Depending on The Iteration Number

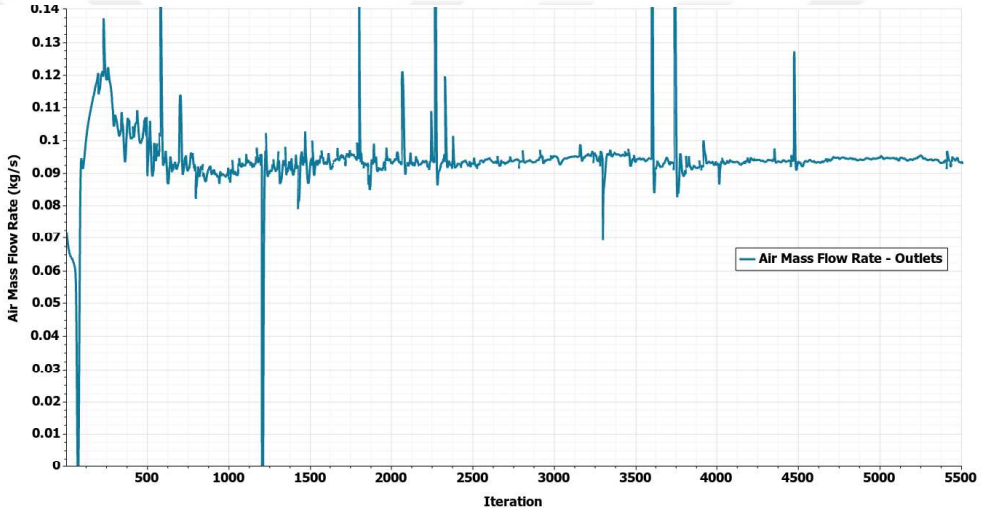

Figure 4.10 Air Outlet Mass Flow Rate Depending on The Iteration Number

Table 4.10 Air Inlet and Outlet Mass Flow Rate Values Depending on the RPM

Rotational Fan Speeds (rpm)	**Air Inlet (kg/s)**	**Air Outlet (kg/s)**
6250	6.18E-02	6.175E-02
9250	9.37-02	9.4E-02
12250	1.24E-02	1.236E-02

All the computational fluid dynamics calculations and experimental results are compared in Table 4.11. Corresponding to the results, the difference between the results is between 0.1 m/s and 4 m/s.

Table 4.11 Comparison of Air Velocity Between CFD and Experimental Results

Air Outlets	CFD Result 6250 rpm	Test Result 6250 rpm	CFD Result 9250 rpm	Test Result 9250 rpm	CFD Result 12250 rpm	Test Result 12250 rpm
1-L	8.1	8.5	13.2	12.7	17.4	17
1-R	9.5	9	14.5	14.3	19.3	19
2-L	7.8	7.6	12.3	11.8	15.1	15.6
2-R	8.1	8.6	11.5	14.2	14.5	18.2
3-L	6.9	7.4	12	11.8	15.1	15.6
3-R	7.2	7	11	11.4	13.3	15.1
4-L	6.2	5.6	7.6	8.4	14	11.5
4-R	6	5.3	8.6	8.3	12.4	11.8
5-L	1.6	1.3	2.3	2.1	7	3
5-R	1.7	1.4	5.6	2.4	3.6	3.1

Moreover, air velocity values, which are differences between measured and calculated values from symmetric air outlets of air distribution ducting, are compared in order to determine the need for air velocity improvement of each air outlet. The air velocity difference at different rotational speeds is investigated in Table 4.12.

Table 4.12 Air Velocity Differences of the Each Air Outlet at Different RPM

	Rotational Fan Speed 6250 rpm		**Rotational Fan Speed 9250 rpm**		**Rotational Fan Speed 12250 rpm**	
	CFD (m/s)	Experimental (m/s)	CFD (m/s)	Experimental (m/s)	CFD (m/s)	Experimental (m/s)
1L-1R	1.4	0.5	1.3	1.6	1.9	2
2L-2R	0.3	1	0.8	2.4	0.6	1.6
3L-3R	0.3	0.4	1	0.4	2	0.5
4L-4R	0.2	0.3	1	0.1	1.6	0.3
5L-5R	0.1	0.1	3.3	0.3	4.1	0.1

Air velocity contours are created as streamline for 6250 rotational fan speeds. The related figures show the swirl motion in the fan zone and air distribution ducting.

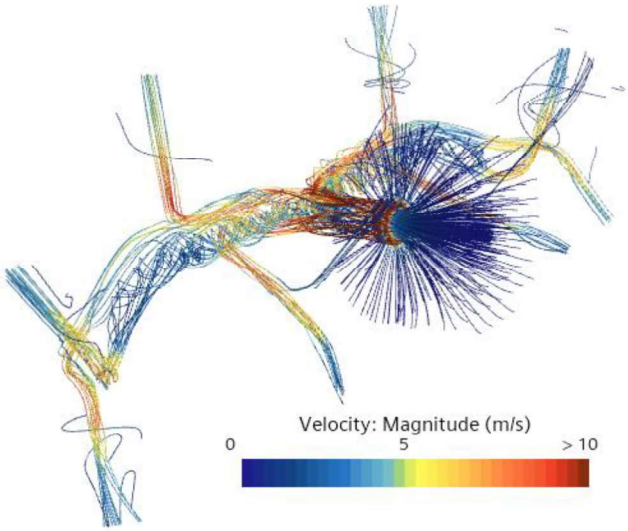

Figure 4.11 Air Velocity Streamlines in the Simulation Model

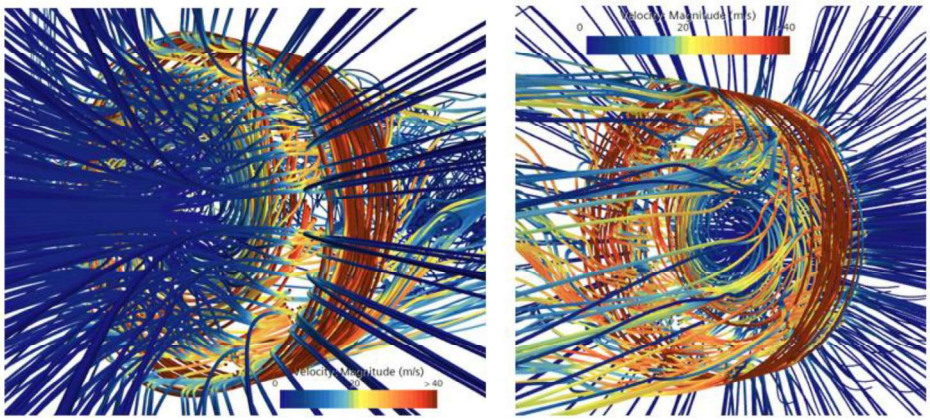

Figure 4.12 Air Velocity Streamlines on The Fan Zones

CHAPTER 5

FLOW DISTRIBUTION IMPROVEMENT STUDY FOR THE DUCTING WITH COMPUTATIONAL METHODS

In this chapter, details of the study performed on the purpose of improving air flow distribution in the air ducting are explained.

5.1 Details of the Straightener Design Study

According to the literature review in Section 2, many different air straightener models were designed and have been used for many years in different industries. The aim of this study is to provide equivalent air flow distribution in symmetric air outlets. Therefore, the same air conditioners are designed and located on the air distribution as symmetric.

A straightener model is created for this air distribution ducting, it is similar with the Zanker plate type straightener. However, our ducting is not a cylindrical duct. Therefore, a special straightener has been developed the inspired by Zanker plate. A new perforated conditioner is shown in Figure 5.1.

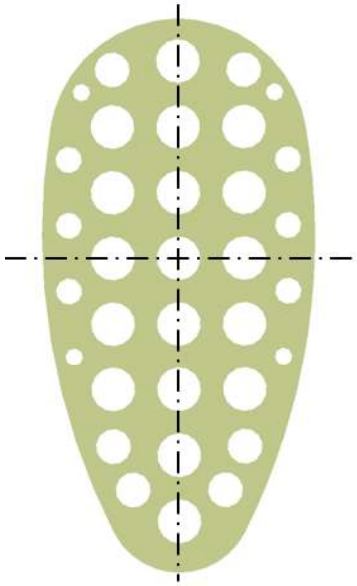

Figure 5.1 A New Designed Air Flow Straightener

The diameter of the holes on the vertical axis and horizontal axis center line is defined as the same. The diameters of the holes are decreased the farther away from the center line like Zanker plate. The smaller holes are concentrated near the plate edge because the major concentration of eddies and swirls is near the wall [15]. Moreover, their diameter, located on the up and low sides of the straightener, is reduced gradually.

To find the optimum hole diameter designed are created three different straighteners, which have different hole diameters. The largest diameter is created as 10 mm, 12 mm, and 14 mm at three different conditioners. According to the studies [6] [15] [20], when the hole diameter is increased, the swirl angle increases. On the other hand, the velocity profile and pressure drop decrease in the ducting. The created straighteners are shown in Figure 5.2, respectively.

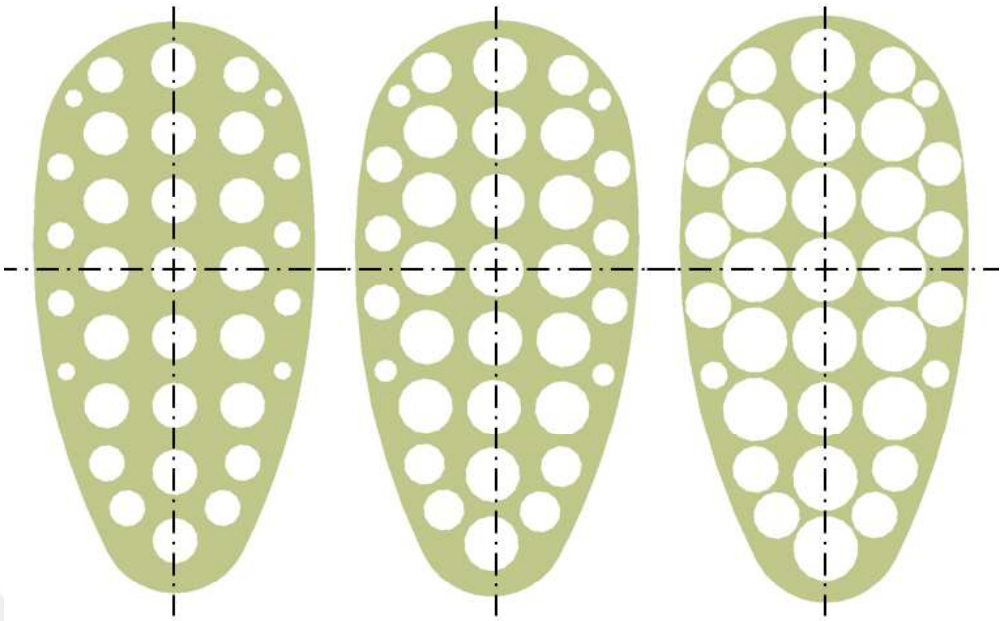

Figure 5.2 The Straighteners at Three Different Hole Sizes

Moreover, three different thicknesses of straighteners are created, which are 4 mm, 6 mm, and 10 mm. One of them is shown in the following figure. We know that the effect of increasing the thickness on the swirl angle, velocity profile and pressure drop is similar with the effects of the increment hole diameter [10 mm, 12 mm, 14 mm]. It could be noted that, the thickness of the straightener cannot be lower than 2 mm since it cannot be produced with composite technology in our company.

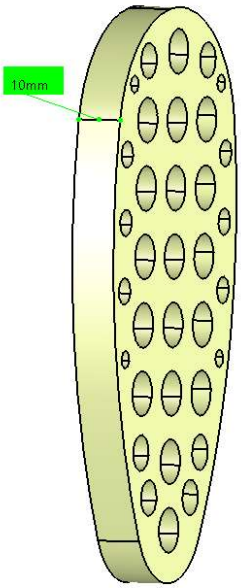

Figure 5.3 The First Conditioner Model at 10 mm Thickness

5.2 Results of the CFD Studies

Totally 9 different geometries, which are at three different hole sizes and three different thicknesses, are created via the 3-D program. The simulations are prepared according to Mesh #2 specifications. The surface and volume mesh of the straightener, that is Model 3 at 10 mm thickness is shown in Figure 5.4.

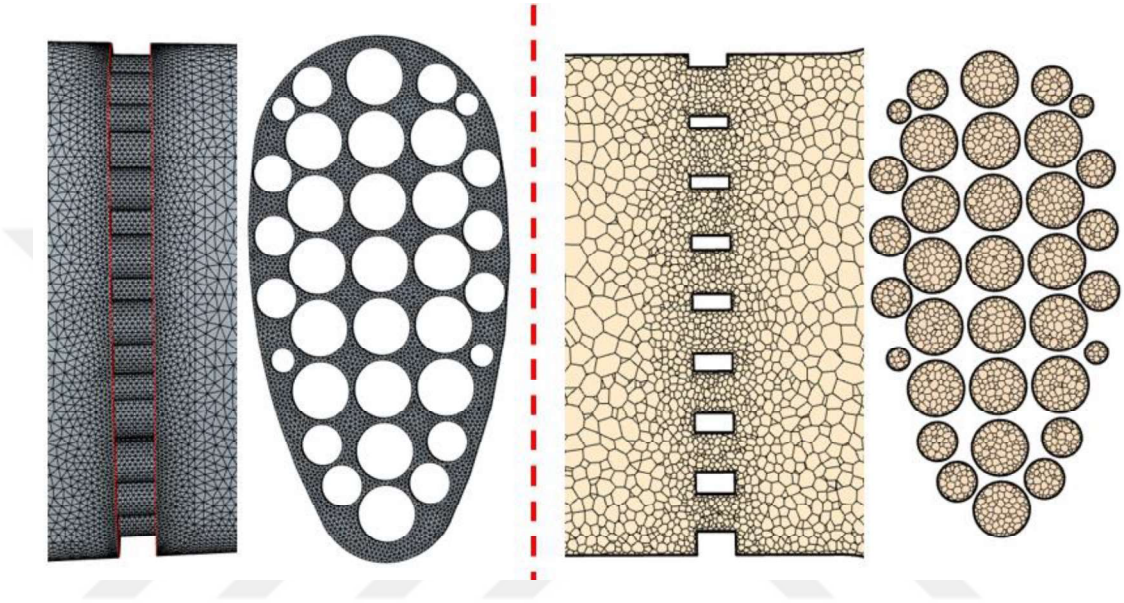

Figure 5.4 Model 3 at 10 mm Thickness Straightener Surface and Volume Mesh

The same boundary conditions are given with the simulations in Section 4. The temperature is taken as a constant value that is 25˚C. The wall is defined as no-slip condition. The simulations are conducted at the three different rotational fan speeds at 6250 rpm, 9250 rpm, and 12250 rpm.

The approximately 25.5 million volume meshes are created in the simulations. The conservation of the mass and velocity profiles are converged at 8000 iterations. A solution takes about approximately 5 hours. Simulations are conducted via cluster and high-performance computing. The 4 nodes and 160 cores are used to the solve simulations.

Point grids are created on the StarCCM+ Derived Part Section to monitor air velocity on the air outlets. CFD result of Model 3 at 10 mm thickness is shown with point grids, which represent are velocity (m/s), for each air outlet at 12250 rpm.

Table 5.1 Air Velocity Distribution on the Each Air Outlet for 12250 rpm

Air Outlets	Left Side Velocity Grids	Right Side Velocity Grids
1	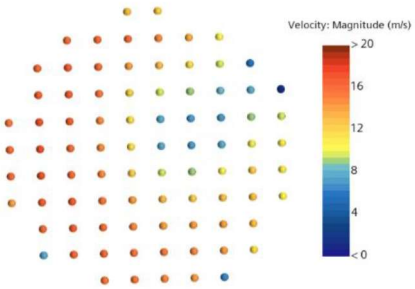	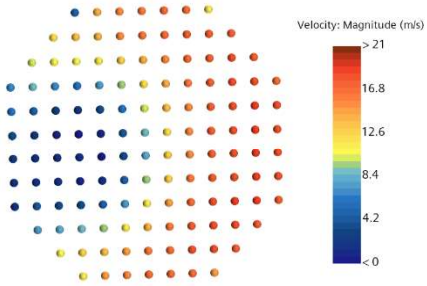
2	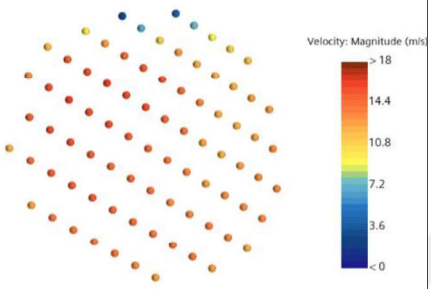	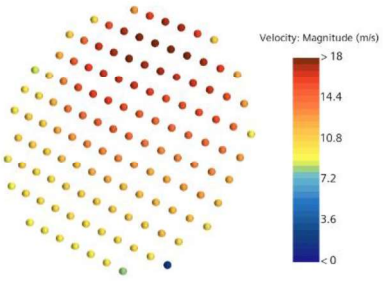
3	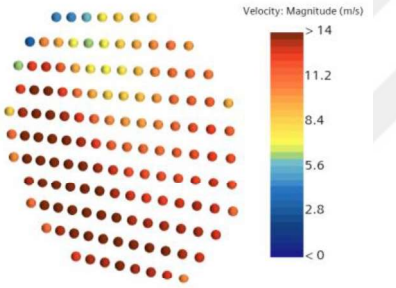	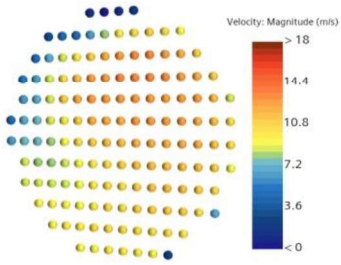
4	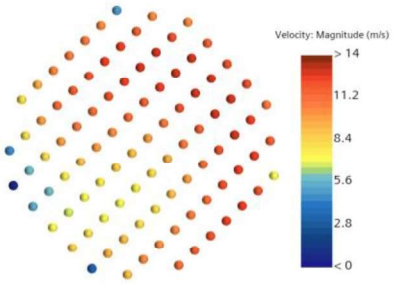	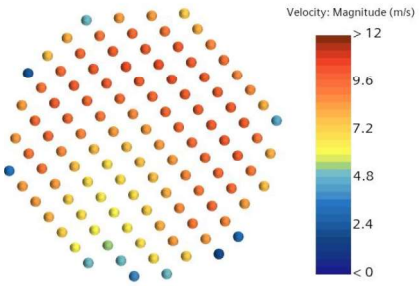
5	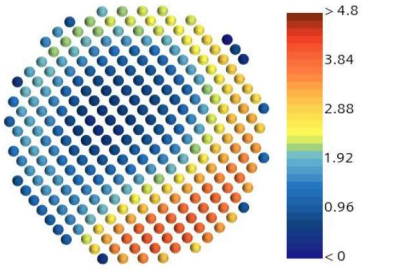	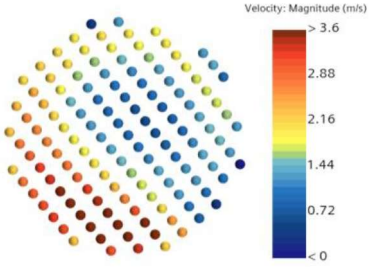

The velocity streamlines from the inlet to the straightener sections are shown at four different maximum velocity scales such as 100 m/s, 50 m/s, 25 m/s, and 12.5 m/s.

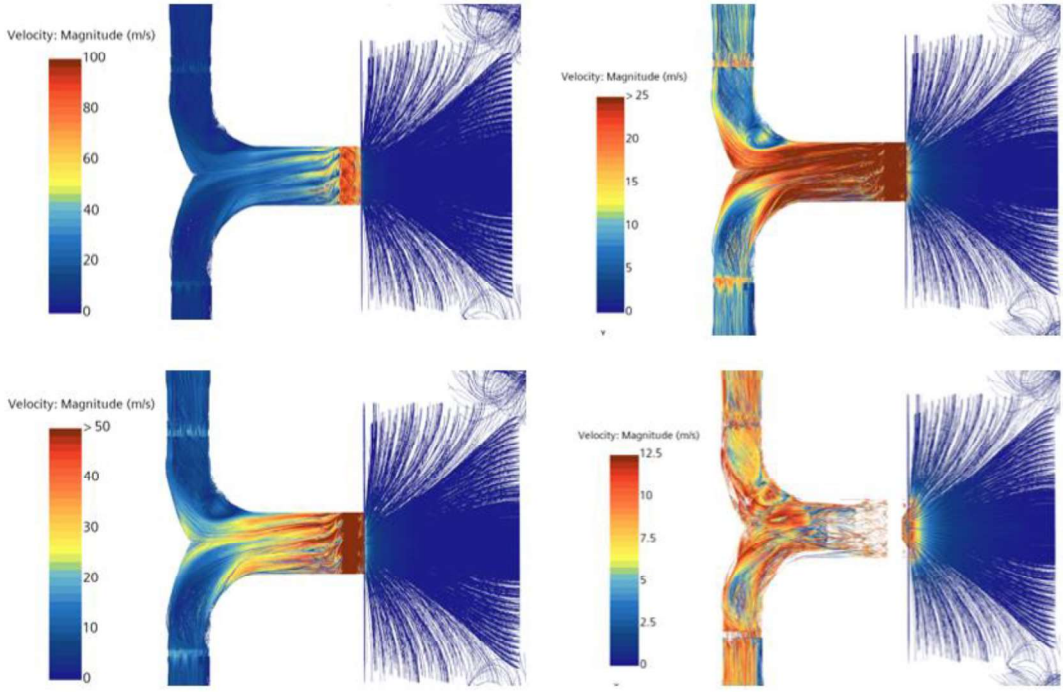

Figure 5.5 Velocity Streamlines at Different Scales of Model 3 with 10 mm

The velocity counter of the left and right-side straighteners is compared in Figure 5.6.

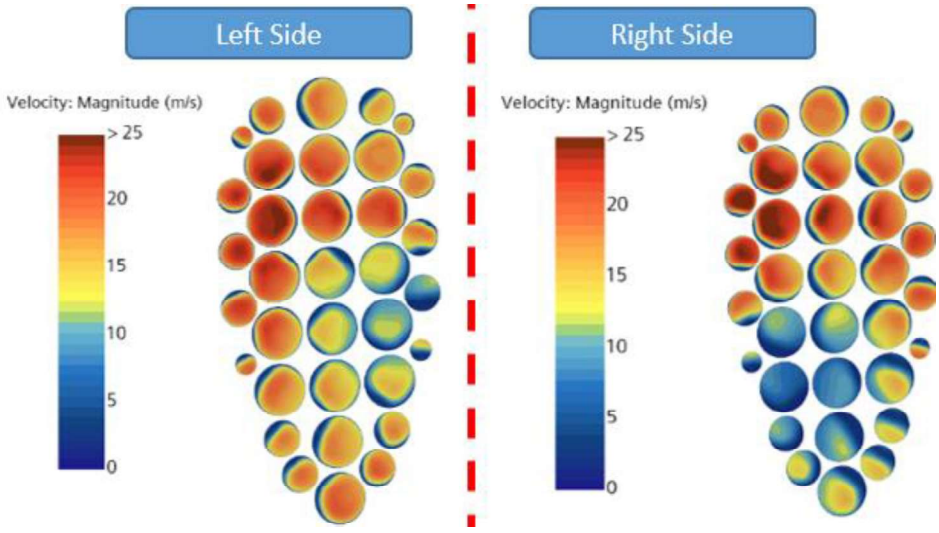

Figure 5.6 Velocity Contour on The Left and Right-Side Straighteners

The total mass flow rate values from the inlet and outlet sections were calculated and compared in order to decide whether the simulation results are true or not. The values are shown in Figure 5.7.

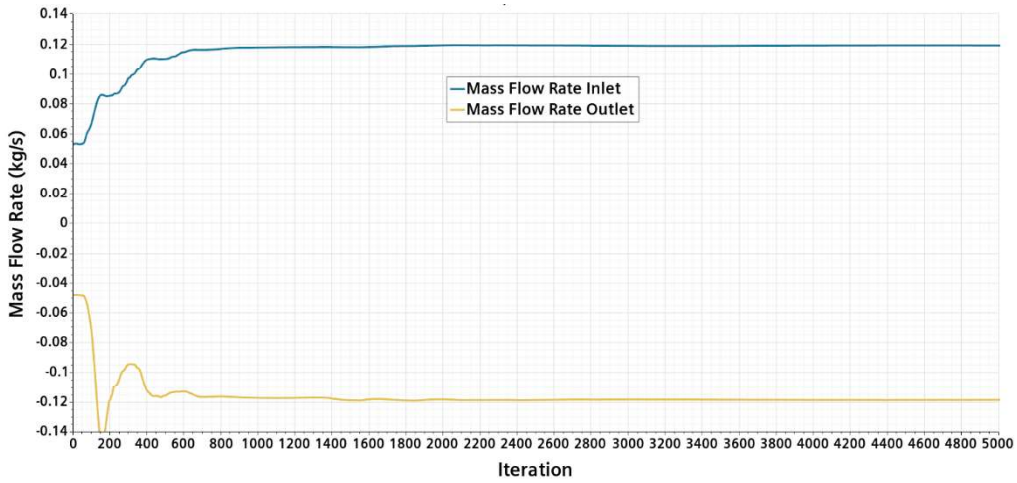

Figure 5.7 Mass Flow Rate Curves at Inlet and Outlet Sections

A total of the twenty-seven simulations are created to investigate air velocity distribution on the air outlet. The velocity improvement for each symmetric air outlets depending on the three different rotational fan speeds, three different straighteners and three different thicknesses are shown in Table 5.2. The negative values show no improvement in the velocity.

Table 5.2 Air Velocity Improvement at Different Rotational Fan Speeds

6250 RPM						
Model ID	**Thickness [mm]**	**1L-1R [m/s]**	**2L-2R [m/s]**	**3L-3R [m/s]**	**4L-4R [m/s]**	**5L-5R [m/s]**
1	**10**	0.65	0	0	0.14	0
	6	-0.9	-0.7	-0.8	0	0.04
	4	-1	-0.7	-0.7	-0.3	0.1
2	**10**	0.4	-0.5	-0.2	-0.2	-0.1
	6	-0.5	-0.6	-0.3	-1.5	-0.7
	4	-1	-0.9	-0.5	-0.8	-0.2
3	**10**	-0.6	-0.7	0.1	-0.6	-0.1
	6	-0.1	-0.1	-0.1	-0.2	-0.7
	4	-0.2	0	-0.1	-1.5	-0.6
9250 RPM						
Model ID	**Thickness [mm]**	**1L-1R [m/s]**	**2L-2R [m/s]**	**3L-3R [m/s]**	**4L-4R [m/s]**	**5L-5R [m/s]**
1	**10**	0.9	0	1	0.7	2.9
	6	1.2	0	0.9	0.9	2.8
	4	0.4	0	0.1	0.9	3.1
2	**10**	0.1	0.2	0.3	0.6	2.5

	6	0	0.6	0.1	0.3	2.2
	4	0	0.6	0	0.2	2.1
3	**10**	-0.5	-0.2	-0.3	-0.1	-0.1
	6	-0.8	-0.6	-0.7	-0.5	-0.1
	4	-0.7	-0.8	-0.7	-0.4	-0.2
12250 RPM						
Model ID	**Thickness [mm]**	**1L-1R [m/s]**	**2L-2R [m/s]**	**3L-3R [m/s]**	**4L-4R [m/s]**	**5L-5R [m/s]**
1	**10**	1.9	0.5	1.4	0.9	2.4
	6	1.9	0.4	1.2	0.9	2.5
	4	1.4	0.2	0.7	0.3	2.3
2	**10**	1.4	0.4	1.2	0.8	1.4
	6	1.0	0.4	0.9	1.1	2.2
	4	0.8	0.4	0.2	1	2
3	**10**	0.2	0	0	0.5	1.7
	6	-0.6	-1	-0.6	-0.8	-0.1
	4	-2.2	-1.2	-0.8	-3.3	-1.2

According to the Table 5.2, four main determinations are deduced, that are listed in the bellowing.

- When the straightener thickness is increased from 4 mm to 10 mm, the velocity improvement is risen. For instance, velocity improvement of Model 1 “3L-LR” at 9250 rpm is risen from 0.1 m/s to 1 m/s when the thickness increased from 4 mm to 10 mm.
- When the straightener hole diameters are increased from the 10 mm (Model 1) to 14 mm (Model 3), the velocity improvement is decreased. For instance, the velocity improvement of Model 1 “1L-1R” with 10 mm thickness at 6250 rpm is 0.65 m/s. The velocity improvement of Model 3 “1L-1R” with 10 mm thickness at 6250 rpm is -0.6 m/s.
- When the rotational fan speed is increased from 6250 rpm to 12250 rpm, the straightener will be more useful with the same straightener model. For example, the average velocity improvement of Model 1 with 10 mm thickness at 6250 rpm is 0.5 m/s. The average velocity improvement of Model 1 with 10 mm thickness at 12250 rpm is 1.5 m/s.

- The larger hole size straightener can be used instead of the thinner straightener for the high rotational fan speeds. For example, for the 12250 rpm, Model 2 with 6 mm thickness at 12 mm hole diameter can be used instead of Model 1 with 6 mm thickness at 10 mm hole diameter.

The left and right-side distribution duct air velocity values are illustrated in Table 5.3. These values are obtained from the only one plane per each side on the simulations.

Table 5.3 Air Velocity of The Left and Right Sides at Different Fan Speeds

		6250 RPM		9250 RPM		12250 RPM	
Model ID	**Thickness [mm]**	**Left [m/s]**	**Right [m/s]**	**Left [m/s]**	**Right [m/s]**	**Left [m/s]**	**Right [m/s]**
1	**10**	3.2	3.5	5.1	5.3	8	7.9
	6	3.5	4	5.7	5.8	8.6	8
	4	3.6	3.8	5.7	6	9.5	8.6
2	**10**	4	4.4	5.8	5.9	8.3	8.5
	6	3.7	4.3	6	6	8	8.1
	4	4	4.4	6.4	6	8.7	8
3	**10**	4.2	4.1	6.6	6	8.6	8
	6	4.2	4.2	6.5	6	8.6	8
	4	4.2	4.3	6.7	6.1	8.7	8.4

The straighteners are used to reduce vortex and to smooth the flow according to the literature survey. The velocity difference between left and right-side air distribution ducts is maximum 0.7 m/s. If the straightener is not used, the velocity difference changes between 1 m/s and 1.5 m/s depends on straightener hole diameter and their thickness.

The mass flow rate values, that are taken for both air inlet and outlet from the CFD simulations, are given for all simulations in Table 5.4.

Table 5.4 The Mass Flow Rate of Air Inlet and Outlet at Different Fan Speeds

		6250 RPM		9250 RPM		12250 RPM	
Model ID	**Thickness [mm]**	**Inlet [g/s]**	**Outlet [g/s]**	**Inlet [g/s]**	**Outlet [g/s]**	**Inlet [g/s]**	**Outlet [g/s]**
1	**10**	43.25	43.13	68.52	68.34	95.66	95.47
	6	43.53	43.46	69.54	69.40	96.49	96.34

	4	43.43	43	69.18	69.02	93.32	93.12
2	**10**	56.51	56.11	84.82	84.59	113.03	112.75
	6	55.86	55.72	83.62	83.45	111.6	111.4
	4	56.11	55.97	84.15	83.97	112.69	112.53
3	**10**	59.66	59.5	89.37	89.17	119.01	118.79
	6	59.76	59.60	89.29	89.04	118.92	118.59
	4	59.66	59.49	89.34	89.07	118.86	118.45

The error is defined as the mass flow rate differences between the air inlet and outlet. During all simulations, the error values are calculated to check simulation accuracy, which is shown in Figure 5.8. According to the simulations, the error maximum is 4.2E-01 g/s. When the rotational fan speed is increased from 6250 rpm to 12250 rpm, the error is risen since the vortexes occur at the high speeds.

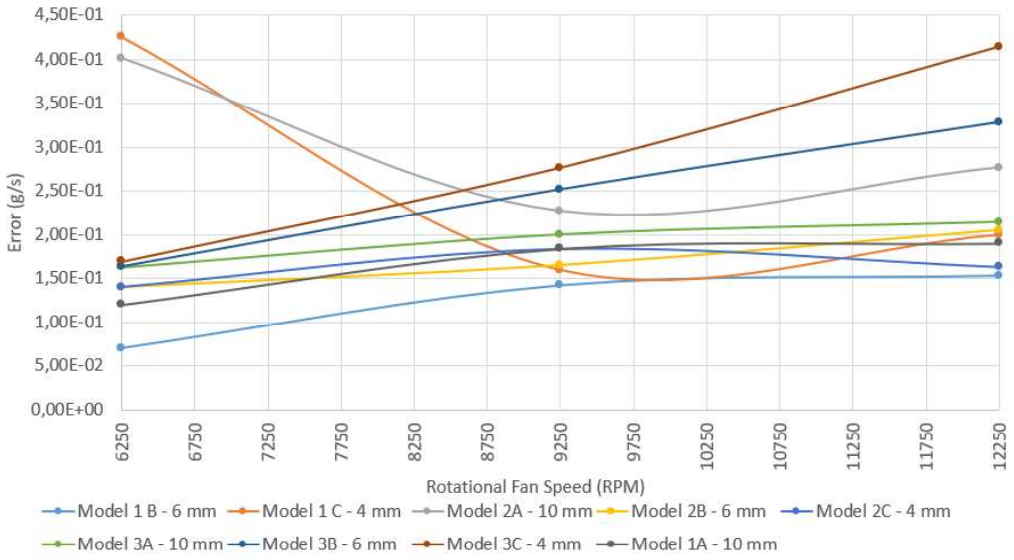

Figure 5.8 The Error as Mass Flow Rate Depending on the Fan Speeds

CHAPTER 6

CONCLUSION AND FUTURE WORKS

Solver is run for 8000 iterations. Around 5000th iteration, it has been seen that air velocity value over the control grids (which is placed at each air outlets) is converged for the cases. The CFD results within the straighteners are presented in Section 5.

According to obtained results, Model 1 with 10 mm thickness can be used to smooth for 6250 rpm since velocity improvements of all air outlets are above the zero. Model 2 with 4 mm thickness can be used to smooth for 9250 rpm since velocity improvements of the vast majority air outlets are above the zero. Model 3 with 10 mm thickness can be used to smooth for 12250 rpm. On the other hand, Model 1 with 10 mm thickness straightener is suggested for 6250 rpm, 9250 rpm and 12250 rpm.

As future works, the effects of different conditioner types, roughness, temperature changes on the air flow distribution in each air outlets are investigated via Star CCM+ or ANSYS Fluent. Moreover, the occurred pressure drop due to the conditioner can be investigated.

REFERENCES

[1] CS-29 Certification Specifications and Acceptable Means of Compliance for Large Rotorcraft

[2] Brennan JA, Sindt CF, Lewis MA, Scott JL (1991). Choosing Flow Conditioners and Their Location for Orifice Flow Measurements. Flow Measurements and Instrumentations 2(1):14–20.

[3] Quazzane AK, Benhadj R (2002). Flow Conditioners Design and Their Effects in Reducing Flow Metering Errors. Sensor Review 22(3):223–231.

[4] Aly, A. A. E., Chong, A., Nicolleau, F., Beck, S., "Experimental study of the pressure drop after fractal-shaped orifices in turbulent pipe flows." Experimental Thermal and Fluid Science 34(1) (2010) :104-111

[5] Brown, G. J., Griffith, B. W., 2013. A New Flow Conditioner for 4-Path Ultrasonic Flowmeters. Paris, France.

[6] Razali, A. H., Nordin, N., Sapit, A., Alias, Z. A., 2020. Flow through Various Porosity of Circle Grid Perforated Plate with Orifice Plate Flowmeter. Journal of Complex Flow, 2(1), 1-6.

[7] Xiong, W., Kalkühler, K., Merzkirch, W., 2003. Velocity and turbulence measurements downstream of flow conditioners. Flow Measurement and Instrumentation, 14(6), 249–260. https://doi.org/10.1016/S0955-5986(03)00031-1

[8] Laribi, B., Wauters, P., Aichouni, M., 2003. Comparative study of aerodynamic behaviour of three flow conditioners. European Journal of Mechanical and Environmental Engineering, 48(1), 21–30.

[9] Pramiyanti, Y., Seri, S. M., Sapit, A., 2020. Incompressible Turbulent Swirling Flow through Circle Grid Perforated Plate. Journal of Complex Flow, 2(1), 11-16.

[10] ISO, 2020. Measurement of fluid flow by means of pressure differential devices inserted in circular cross-section conduits running full-Part 2: Orifice plates (EN ISO 5167-3). European Committee for Standardization, Technical Procedure.

[11] Chen, G., Liu, G., 2018. Performance Evaluation and Analysis of a New Flow Conditioner Based on CFD. IOP Conference Series: Materials Science and Engineering, 394, 032049. https://doi.org/10.1088/1757-899X/394/3/032049

[12] Zaryankin, A., Rogalev, N., Rogalev, A., Kocherova, A., Kurdiukova, G., 2016. New Flow Stabilizers as a Method to Improve the Reliability and Efficiency of Power Equipment. Modern Applied Science,10(2),172-184. https://doi.org/10.5539/mas.v10n2p172.

[13] Gordeev S, Gröschel F, Heinzel V, et al. Numerical study of the flow conditioner for the IFMIF liquid lithium target [J]. *Fusion Eng Des*, **2014**, 89 (7): 1751-1757.

[14] Drainy, Y. A. E., Saqr, K. M., Aly, H. S. and Jaafar, M. N. M., (2009) CFD analysis of Incompressible Turbulent Swirling Flow Trough Zanker Plate, Engineering Applications of Computational Fluid Mechanics Vol. 3, No. 4, pp. 562–572.

[15] Ahmet Çağrı Bilir, Ali Doğrul, Nurten Vardar, 2022, AN EXTENSIVE INVESTIGATION OF FLOW CONDITIONERS INSIDE A FI-FI MONITOR, 681.533.38:621.184.22, http://dx.doi.org/10.21278/brod73408.

[16] Miller, R. W., 1996. Flow Measurement Engineering Handbook, 3rd edition: McGraw-Hill.

[17] Crabtree, M. A. (2009), Industrial Flow Measurement, degree of Master of Science by Research, University of Huddersfield, West Yorkshire, England.

[18] Baker RC (2000). Flow Measurement Handbook: Industrial Designs, Operating Principles, Performance and Applications, Cambridge University Press, 27–30.

[19] Askari, V., Nicolas, D., Edralin, M., Jang, C., 2019. Computational Fluid Dynamics Model for Sensitivity Analysis and Design of Flow Conditioners. Proceedings of the 9th International Conference on Simulation and Modeling Methodologies, Technologies and Applications, Prague, Czech Republic. https://doi.org/10.5220/0007917401290140.

[20] Bayazit, Y., Sparrow, E. M., Joseph, D. D., 2014. Perforated plates for fluid management: Plate geometry effects and flow regimes. International Journal of Thermal Science, 85, 104–111. https://doi.org/10.1016/j.ijthermalsci.2014.06.002

[21] Çarpınlıoğlu, M. Ö., Özahi, E., 2011. Laminar flow control via utilization of pipe entrance inserts (a comment on entrance length concept). Flow Measurement and Instrumentation, 22(3), 165–174.https://doi.org/10.1016/j.flowmeasinst.2011.01.005.

[22] Manshoor, B., Nicolleau, F. C. G. A., Beck, S. B. M., "The fractal flow conditioner for orifice plate flow meters." Flow Measurement and Instrumentation 22 (2011) pp.208–214.

[23] Vaidya, H. A., Ertunc, O., Genc, B., Beyer, F., Koksoy, C. & Delgado, A., "Numerical simulations of swirling pipe decay of swirl and occurrence of vortex structures." Journal of Physics: Conference Series 318 (2011).

[24] Lahadi, M. H., Johari, A. M., Alias, Z. A., 2019. Effect of the Fractal-Grid Generated Turbulence on Turbulent Intensity and Pressure Drop in Pipe Flow. Journal of Complex Flow, 1(1), 5-10.

[25] Instructions for use, Schmidt Technology Flow Sensor SS 20.260, Version 508981.02G

[26] *Tennekes, H.; Lumley, J. L. (1992). A first course in turbulence (14. print. ed.). Cambridge, Mass. [u.a.]: MIT Press.* ISBN 978-0-262-20019-6.

[27] *Star CCM+, Incs, 13.06.012-R8 Theory Guide, 2018.*

[28] Menter, Florian R. "Improved two-equation k-omega turbulence models for aerodynamic flows." (1992).

[29] ANSYS, Inc, *ANSYS Fluent 15.0 Theory Guide,* 2013.

[30] On self-propulsion assessment of marine vehicles, Abdi Kukner's Lab, October 2018, Brodogradnja 69(4):29-51, Omer Kemal Kinaci,Metin Kemal Gokce

[31] You, W. Liu, J. Chen, C.-H. Lin, D. Wei and Q. Chen, "Predicting airflow distribution and contaminant transport in aircraft cabins with a simplified gasper model," Building Performance Simulation, vol. 9, no. 6, pp. 699-708, June 2016.

[32] ANSI/AMCA210-07, Laboratory Methods of Testing Fans for Certified Aerodynamic.

[33] Doruk Sahin, Analysis of flow structure in a helicopter cabin to improve the thermal comfort using computational fluid dynamics modeling, METU,2018,

[34] Menter, F. R., 1993. Zonal Two Equation k-omega Turbulence Models for Aerodynamic Flows. *23rd AIAA Fluid Dynamics, Plasmadynamics and Lasers Conference*, Orlando, Florida, USA. https://doi.org/10.2514/6.1993-2906

[35] Menter, F. R., 1994. Two-Equation Eddy-Viscosity Turbulence Models for Engineering Applications. *AIAA J.*, 32(8), 1598-1605. https://doi.org/10.2514/3.12149

APPENDICES

Appendix A: Mesh Quality Properties of Mesh#1

Appendix B: Mesh Quality Properties of Mesh#2

Appendix C: Mesh Quality Properties of Mesh#3

Appendix A – Mesh Quality Properties of Mesh#1

The simulations consist of three different regions such as ducting fluid volume, ventilation fan fluid volume, and inlet volume. Mesh quality of Mesh#1 are shown in the below for each region. Additionally, the overall statistics values are given.

```
------------------------------------------------------
--- Computing statistics in Region: Ducting Fluid Volume
------------------------------------------------------
-> ENTITY COUNT:
   # Cells: 9783097
   # Faces: 41350788
   # Verts: 23245300
-> EXTENTS:
   x: [ 1.7222e+00,  2.4959e+00] m
   y: [-1.0269e+00,  1.0269e+00] m
   z: [ 1.2054e+00,  2.0261e+00] m
-> MESH VALIDITY:
   Mesh is topologically valid and has no negative volume cells.
-> FACE VALIDITY STATISTICS:
Minimum Face Validity: 9.365750e-01
Maximum Face Validity: 1.000000e+00
        Face Validity <  0.50           0    0.000%
0.50 <= Face Validity <  0.60           0    0.000%
0.60 <= Face Validity <  0.70           0    0.000%
0.70 <= Face Validity <  0.80           0    0.000%
0.80 <= Face Validity <  0.90           0    0.000%
0.90 <= Face Validity <  0.95           4    0.000%
0.95 <= Face Validity <  1.00          60    0.001%
1.00 <= Face Validity            9783033   99.999%
-> VOLUME CHANGE STATISTICS:
Minimum Volume Change: 5.544557e-03
Maximum Volume Change: 1.000000e+00
         Volume Change <  0e+00         0    0.000%
0e+00 <= Volume Change <  1e-06         0    0.000%
1e-06 <= Volume Change <  1e-05         0    0.000%
1e-05 <= Volume Change <  1e-04         0    0.000%
1e-04 <= Volume Change <  1e-03         0    0.000%
1e-03 <= Volume Change <  1e-02         1    0.000%
1e-02 <= Volume Change <  1e-01    187628    1.918%
1e-01 <= Volume Change <= 1e+00   9595468   98.082%
------------------------------------------------------
    ------------------------------------------------------
    --- Computing statistics in Region: Inlet - Plenum
    ------------------------------------------------------
    -> ENTITY COUNT:
       # Cells: 75328
       # Faces: 498255
       # Verts: 447164
    -> EXTENTS:
       x: [ 1.9148e+00,  2.3152e+00] m
       y: [-2.2494e-01,  2.2499e-01] m
       z: [ 1.1972e+00,  1.7080e+00] m
    -> MESH VALIDITY:
       Mesh is topologically valid and has no negative volume cells.
    -> FACE VALIDITY STATISTICS:
    Minimum Face Validity: 1.000000e+00
    Maximum Face Validity: 1.000000e+00
            Face Validity <  0.50           0    0.000%
    0.50 <= Face Validity <  0.60           0    0.000%
    0.60 <= Face Validity <  0.70           0    0.000%
    0.70 <= Face Validity <  0.80           0    0.000%
    0.80 <= Face Validity <  0.90           0    0.000%
    0.90 <= Face Validity <  0.95           0    0.000%
    0.95 <= Face Validity <  1.00           0    0.000%
    1.00 <= Face Validity              75328  100.000%
    -> VOLUME CHANGE STATISTICS:
    Minimum Volume Change: 1.183220e-02
    Maximum Volume Change: 1.000000e+00
             Volume Change <  0e+00         0    0.000%
    0e+00 <= Volume Change <  1e-06         0    0.000%
    1e-06 <= Volume Change <  1e-05         0    0.000%
    1e-05 <= Volume Change <  1e-04         0    0.000%
    1e-04 <= Volume Change <  1e-03         0    0.000%
    1e-03 <= Volume Change <  1e-02         0    0.000%
    1e-02 <= Volume Change <  1e-01      3028    4.020%
    1e-01 <= Volume Change <= 1e+00     72300   95.980%
```

```
------------------------------------------------------
--- Computing statistics in Region: Ventilation Fan Fluid Volume - Rotating
------------------------------------------------------
-> ENTITY COUNT:
   # Cells: 12763411
   # Faces: 52905070
   # Verts: 28914670
-> EXTENTS:
   x: [ 1.9474e+00,  2.0174e+00] m
   y: [-4.8911e-02,  4.8967e-02] m
   z: [ 1.4540e+00,  1.5583e+00] m
-> MESH VALIDITY:
   Mesh is topologically valid and has no negative volume cells.
-> FACE VALIDITY STATISTICS:
Minimum Face Validity: 8.158344e-01
Maximum Face Validity: 1.000000e+00
        Face Validity <  0.50           0    0.000%
0.50 <= Face Validity <  0.60           0    0.000%
0.60 <= Face Validity <  0.70           0    0.000%
0.70 <= Face Validity <  0.80           0    0.000%
0.80 <= Face Validity <  0.90           5    0.000%
0.90 <= Face Validity <  0.95         423    0.003%
0.95 <= Face Validity <  1.00        2273    0.018%
1.00 <= Face Validity            12760710   99.979%
-> VOLUME CHANGE STATISTICS:
Minimum Volume Change: 4.398168e-05
Maximum Volume Change: 1.000000e+00
         Volume Change <  0e+00           0    0.000%
0e+00 <= Volume Change <  1e-06           0    0.000%
1e-06 <= Volume Change <  1e-05           0    0.000%
1e-05 <= Volume Change <  1e-04           5    0.000%
1e-04 <= Volume Change <  1e-03         230    0.002%
1e-03 <= Volume Change <  1e-02        2303    0.018%
1e-02 <= Volume Change <  1e-01      222016    1.739%
1e-01 <= Volume Change <= 1e+00    12538857   98.241%
------------------------------------------------------
--- Overall Statistics:
------------------------------------------------------
-> ENTITY COUNT:
   # Cells: 22621836
   # Faces: 94754113
   # Verts: 52607134
-> MESH VALIDITY:
   Mesh is topologically valid and has no negative volume cells.
-> FACE VALIDITY STATISTICS:
Minimum Face Validity: 8.158344e-01
Maximum Face Validity: 1.000000e+00
        Face Validity <  0.50           0    0.000%
0.50 <= Face Validity <  0.60           0    0.000%
0.60 <= Face Validity <  0.70           0    0.000%
0.70 <= Face Validity <  0.80           0    0.000%
0.80 <= Face Validity <  0.90           5    0.000%
0.90 <= Face Validity <  0.95         427    0.002%
0.95 <= Face Validity <  1.00        2333    0.010%
1.00 <= Face Validity            22619071   99.988%
-> VOLUME CHANGE STATISTICS:
Minimum Volume Change: 4.398168e-05
Maximum Volume Change: 1.000000e+00
         Volume Change <  0e+00           0    0.000%
0e+00 <= Volume Change <  1e-06           0    0.000%
1e-06 <= Volume Change <  1e-05           0    0.000%
1e-05 <= Volume Change <  1e-04           5    0.000%
1e-04 <= Volume Change <  1e-03         230    0.001%
1e-03 <= Volume Change <  1e-02        2304    0.010%
1e-02 <= Volume Change <  1e-01      412672    1.824%
1e-01 <= Volume Change <= 1e+00    22206625   98.165%
```

Appendix B – Mesh Quality Properties of Mesh#2

The simulations consist of three different regions such as ducting fluid volume, ventilation fan fluid volume, and inlet volume. Mesh quality of Mesh#2 are shown in the below for each region. Additionally, the overall statistics values are given.

```
--- Computing statistics in Region: Ducting Fluid Volume

-> ENTITY COUNT:
   # Cells: 12604025
   # Faces: 53892188
   # Verts: 30832435

-> FACE VALIDITY STATISTICS:
Minimum Face Validity: 9.308557e-01
Maximum Face Validity: 1.000000e+00
        Face Validity <  0.50           0    0.000%
0.50 <= Face Validity <  0.60           0    0.000%
0.60 <= Face Validity <  0.70           0    0.000%
0.70 <= Face Validity <  0.80           0    0.000%
0.80 <= Face Validity <  0.90           0    0.000%
0.90 <= Face Validity <  0.95           5    0.000%
0.95 <= Face Validity <  1.00          64    0.001%
1.00 <= Face Validity           12603956   99.999%

-> VOLUME CHANGE STATISTICS:
Minimum Volume Change: 6.329361e-03
Maximum Volume Change: 1.000000e+00
         Volume Change <  0e+00         0    0.000%
0e+00 <= Volume Change <  1e-06         0    0.000%
1e-06 <= Volume Change <  1e-05         0    0.000%
1e-05 <= Volume Change <  1e-04         0    0.000%
1e-04 <= Volume Change <  1e-03         0    0.000%
1e-03 <= Volume Change <  1e-02         2    0.000%
1e-02 <= Volume Change <  1e-01    257280    2.041%
1e-01 <= Volume Change <= 1e+00   12346743   97.959%
```

```
--- Computing statistics in Region: Inlet - Plenum

-> ENTITY COUNT:
   # Cells: 121640
   # Faces: 805218
   # Verts: 722361

-> FACE VALIDITY STATISTICS:
Minimum Face Validity: 1.000000e+00
Maximum Face Validity: 1.000000e+00
        Face Validity <  0.50           0    0.000%
0.50 <= Face Validity <  0.60           0    0.000%
0.60 <= Face Validity <  0.70           0    0.000%
0.70 <= Face Validity <  0.80           0    0.000%
0.80 <= Face Validity <  0.90           0    0.000%
0.90 <= Face Validity <  0.95           0    0.000%
0.95 <= Face Validity <  1.00           0    0.000%
1.00 <= Face Validity              121640  100.000%

-> VOLUME CHANGE STATISTICS:
Minimum Volume Change: 1.115442e-02
Maximum Volume Change: 1.000000e+00
         Volume Change <  0e+00         0    0.000%
0e+00 <= Volume Change <  1e-06         0    0.000%
1e-06 <= Volume Change <  1e-05         0    0.000%
1e-05 <= Volume Change <  1e-04         0    0.000%
1e-04 <= Volume Change <  1e-03         0    0.000%
1e-03 <= Volume Change <  1e-02         0    0.000%
1e-02 <= Volume Change <  1e-01      5071    4.169%
1e-01 <= Volume Change <= 1e+00    116569   95.831%
```

```
--- Computing statistics in Region: Ventilation Fan Fluid Volume - Rotating

-> ENTITY COUNT:
   # Cells: 12762298
   # Faces: 52099258
   # Verts: 28910206

-> FACE VALIDITY STATISTICS:
Minimum Face Validity: 8.866022e-01
Maximum Face Validity: 1.000000e+00
        Face Validity <  0.50           0    0.000%
0.50 <= Face Validity <  0.60           0    0.000%
0.60 <= Face Validity <  0.70           0    0.000%
0.70 <= Face Validity <  0.80           0    0.000%
0.80 <= Face Validity <  0.90           5    0.000%
0.90 <= Face Validity <  0.95         470    0.004%
0.95 <= Face Validity <  1.00        2208    0.017%
1.00 <= Face Validity           12759615   99.979%

-> VOLUME CHANGE STATISTICS:
Minimum Volume Change: 2.441304e-05
Maximum Volume Change: 1.000000e+00
         Volume Change <  0e+00         0    0.000%
0e+00 <= Volume Change <  1e-06         0    0.000%
1e-06 <= Volume Change <  1e-05         0    0.000%
1e-05 <= Volume Change <  1e-04         7    0.000%
1e-04 <= Volume Change <  1e-03       274    0.002%
1e-03 <= Volume Change <  1e-02      2600    0.020%
1e-02 <= Volume Change <  1e-01    225472    1.767%
1e-01 <= Volume Change <= 1e+00   12533945   98.211%
```

```
--- Overall Statistics:

-> ENTITY COUNT:
   # Cells: 25487963
   # Faces: 107596664
   # Verts: 60465002
-> MESH VALIDITY:
   Mesh is topologically valid and has no negative volume cells.
-> FACE VALIDITY STATISTICS:
Minimum Face Validity: 8.866022e-01
Maximum Face Validity: 1.000000e+00
        Face Validity <  0.50           0    0.000%
0.50 <= Face Validity <  0.60           0    0.000%
0.60 <= Face Validity <  0.70           0    0.000%
0.70 <= Face Validity <  0.80           0    0.000%
0.80 <= Face Validity <  0.90           5    0.000%
0.90 <= Face Validity <  0.95         475    0.002%
0.95 <= Face Validity <  1.00        2272    0.009%
1.00 <= Face Validity           25485211   99.989%
-> VOLUME CHANGE STATISTICS:
Minimum Volume Change: 2.441304e-05
Maximum Volume Change: 1.000000e+00
         Volume Change <  0e+00         0    0.000%
0e+00 <= Volume Change <  1e-06         0    0.000%
1e-06 <= Volume Change <  1e-05         0    0.000%
1e-05 <= Volume Change <  1e-04         7    0.000%
1e-04 <= Volume Change <  1e-03       274    0.001%
1e-03 <= Volume Change <  1e-02      2602    0.010%
1e-02 <= Volume Change <  1e-01    487823    1.914%
1e-01 <= Volume Change <= 1e+00   24997257   98.075%
```

Appendix C – Mesh Quality Properties of Mesh#3

The simulations consist of three different regions such as ducting fluid volume, ventilation fan fluid volume, and inlet volume. Mesh quality of Mesh#3 are shown in the below for each region. Additionally, the overall statistics values are given.

```
-----------------------------------------------------
--- Computing statistics in Region: Ducting Fluid Volume
-----------------------------------------------------
-> ENTITY COUNT:
   # Cells: 15079900
   # Faces: 65163210
   # Verts: 37856046
-> EXTENTS:
   x: [ 1.7222e+00,  2.4959e+00] m
   y: [-1.0269e+00,  1.0270e+00] m
   z: [ 1.2053e+00,  2.0261e+00] m
-> MESH VALIDITY:
   Mesh is topologically valid and has no negative volume cells.
-> FACE VALIDITY STATISTICS:
Minimum Face Validity: 9.450824e-01
Maximum Face Validity: 1.000000e+00
        Face Validity <  0.50            0    0.000%
0.50 <= Face Validity <  0.60            0    0.000%
0.60 <= Face Validity <  0.70            0    0.000%
0.70 <= Face Validity <  0.80            0    0.000%
0.80 <= Face Validity <  0.90            0    0.000%
0.90 <= Face Validity <  0.95            1    0.000%
0.95 <= Face Validity <  1.00           11    0.000%
1.00 <= Face Validity             15079888  100.000%
-----------------------------------------------------
--- Computing statistics in Region: Ventilation Fan Fluid Volume - Rotating
-----------------------------------------------------
-> ENTITY COUNT:
   # Cells: 14401033
   # Faces: 60011678
   # Verts: 32993093
-> EXTENTS:
   x: [ 1.9474e+00,  2.0174e+00] m
   y: [-4.8913e-02,  4.8968e-02] m
   z: [ 1.4540e+00,  1.5583e+00] m
-> MESH VALIDITY:
   Mesh is topologically valid and has no negative volume cells.
-> FACE VALIDITY STATISTICS:
Minimum Face Validity: 8.651374e-01
Maximum Face Validity: 1.000000e+00
        Face Validity <  0.50            0    0.000%
0.50 <= Face Validity <  0.60            0    0.000%
0.60 <= Face Validity <  0.70            0    0.000%
0.70 <= Face Validity <  0.80            0    0.000%
0.80 <= Face Validity <  0.90            8    0.000%
0.90 <= Face Validity <  0.95          375    0.003%
0.95 <= Face Validity <  1.00         1688    0.012%
1.00 <= Face Validity             14398962   99.986%
-> VOLUME CHANGE STATISTICS:
Minimum Volume Change: 1.908131e-05
Maximum Volume Change: 1.000000e+00
         Volume Change <  0e+00          0    0.000%
0e+00 <= Volume Change <  1e-06          0    0.000%
1e-06 <= Volume Change <  1e-05          0    0.000%
1e-05 <= Volume Change <  1e-04          3    0.000%
1e-04 <= Volume Change <  1e-03        164    0.001%
1e-03 <= Volume Change <  1e-02       1777    0.012%
1e-02 <= Volume Change <  1e-01     213618    1.483%
1e-01 <= Volume Change <= 1e+00   14185471   98.503%
-----------------------------------------------------
-----------------------------------------------------
--- Computing statistics in Region: Inlet - Plenum
-----------------------------------------------------
-> ENTITY COUNT:
   # Cells: 295610
   # Faces: 1961495
   # Verts: 1757463
-> EXTENTS:
   x: [ 1.9148e+00,  2.3152e+00] m
   y: [-2.2497e-01,  2.2502e-01] m
   z: [ 1.1971e+00,  1.7080e+00] m
-> MESH VALIDITY:
   Mesh is topologically valid and has no negative volume cells.
-> FACE VALIDITY STATISTICS:
Minimum Face Validity: 1.000000e+00
Maximum Face Validity: 1.000000e+00
        Face Validity <  0.50            0    0.000%
0.50 <= Face Validity <  0.60            0    0.000%
0.60 <= Face Validity <  0.70            0    0.000%
0.70 <= Face Validity <  0.80            0    0.000%
0.80 <= Face Validity <  0.90            0    0.000%
0.90 <= Face Validity <  0.95            0    0.000%
0.95 <= Face Validity <  1.00            0    0.000%
1.00 <= Face Validity              295610  100.000%
-> VOLUME CHANGE STATISTICS:
Minimum Volume Change: 1.105081e-02
Maximum Volume Change: 1.000000e+00
         Volume Change <  0e+00          0    0.000%
0e+00 <= Volume Change <  1e-06          0    0.000%
1e-06 <= Volume Change <  1e-05          0    0.000%
1e-05 <= Volume Change <  1e-04          0    0.000%
1e-04 <= Volume Change <  1e-03          0    0.000%
1e-03 <= Volume Change <  1e-02          0    0.000%
1e-02 <= Volume Change <  1e-01      10801    3.654%
1e-01 <= Volume Change <= 1e+00     284809   96.346%
-----------------------------------------------------
--- Overall Statistics:
-----------------------------------------------------
-> ENTITY COUNT:
   # Cells: 29776543
   # Faces: 127136383
   # Verts: 72606602
-> MESH VALIDITY:
   Mesh is topologically valid and has no negative volume cells.
-> FACE VALIDITY STATISTICS:
Minimum Face Validity: 8.651374e-01
Maximum Face Validity: 1.000000e+00
        Face Validity <  0.50            0    0.000%
0.50 <= Face Validity <  0.60            0    0.000%
0.60 <= Face Validity <  0.70            0    0.000%
0.70 <= Face Validity <  0.80            0    0.000%
0.80 <= Face Validity <  0.90            8    0.000%
0.90 <= Face Validity <  0.95          376    0.001%
0.95 <= Face Validity <  1.00         1699    0.006%
1.00 <= Face Validity             29774460   99.993%
-> VOLUME CHANGE STATISTICS:
Minimum Volume Change: 1.908131e-05
Maximum Volume Change: 1.000000e+00
         Volume Change <  0e+00          0    0.000%
0e+00 <= Volume Change <  1e-06          0    0.000%
1e-06 <= Volume Change <  1e-05          0    0.000%
1e-05 <= Volume Change <  1e-04          3    0.000%
1e-04 <= Volume Change <  1e-03        164    0.001%
1e-03 <= Volume Change <  1e-02       1778    0.006%
1e-02 <= Volume Change <  1e-01     657874    2.209%
1e-01 <= Volume Change <= 1e+00   29116724   97.784%
```